THE CRYSTALLIZATION BEHAVIOUR OF ISOTACTIC POLYBUTENE-1

A THESIS SUBMITTED TO
THE DEPARTMENT OF CHEMISTRY
AND THE INSTITUTE OF ENGINEERING AND SCIENCE OF
BILKENT UNIVERSITY
IN PARTIAL FULFILLMENT OF THE REQUIREMENTS
FOR THE DEGREE OF MASTER OF SCIENCE

BY

HACI BAYRAM ERDEM

AUGUST 2002

I certify that I read this thesis and that in my opinion it is fully adequate, in scope and in quality, as a thesis for the degree of Master of Science.

_____

Asst. Prof. Dr. Gürhan Kalay (Supervisor)

I certify that I read this thesis and that in my opinion it is fully adequate, in scope and in quality, as a thesis for the degree of Master of Science.

_____

Prof. Dr. Şefik Süzer

I certify that I read this thesis and that in my opinion it is fully adequate, in scope and in quality, as a thesis for the degree of Master of Science.

_____

Assoc. Prof. Dr. C. Hakan Gür

Approved for Institute of Engineering and Science.

_____

Prof. Dr. Mehmet Baray

Director of Institute of Engineering and Science

ABSTRACT

THE CRYSTALLIZATION BEHAVIOUR OF ISOTACTIC POLYBUTENE-1

Haci Bayram Erdem

M.S in Chemistry

Supervisor: Assist. Prof. Dr. Gürhan Kalay

August 2002

The crystallization behaviour of different commercial grades of isotactic polybutene-1 was investigated and an experimental set-up was designed for this research study. The experimental set-up constructed provides both fast-cooling of the sample and the recording of the growth of spherulites as a real time movie. The radial growth rate of the spherulites were observed to be higher for the grades with higher molecular weights. The results were found to fit to the Lauritzenn-Hoffman crystallization theory, and this theory is used to calculate the lateral surface free energy, σ, and fold surface free energy, σ_e. The lateral surface free energy was found to be 10.4 erg/cm^2 for all the grades investigated. The fold surface free energy calculated to be between 15.5 to 17.4 erg/cm^2. The fold surface free energies and the crystallization rates do not exhibit any dependence on the molecular weight of the polymer. The polymer containing nucleating agents has the highest crystallization rate. It was observed that the likelihood of deviation from spherical shape is greater for the grades with lower molecular weights.

Key-words :polybutene-1, Lauritzen-Hoffman theory, spherulite growth rate, nucleating agent, crystallization rate, polymer crystallization

ÖZET

İZOTAKTİK POLİBÜTEN-1'İN KRİSTALLEŞME DAVRANIŞI

Hacı Bayram Erdem
Kimya Yüksek Lisans
Tez Yöneticisi: Assist. Prof. Dr. Gürhan Kalay
Ağustos 2002

Polibuten-1'in dört farklı ticari türünün kristalleşme davranışı incelendi ve bu inceleme için bir deney düzeneği hazırlandı. Hazırlanan deney düzeneği, aynı zamanda numunelerin hızlı-soğutulmasını ve küresel kristal yapıların büyümesini gerçek zamanlı bir film olarak kaydedilmesini sağladı. Yarıçapsal büyüme hızlarının, büyük molekül ağırlıklı sınıflar için daha büyük olduğu gözlemlendi. Bulunan sonuçların Lauritzen-Hoffman kristalleşme teorisine uygunluğu gösterildi ve bu teori yanal yüzey serbest enerjisi, σ, ile katlanma yüzeyi serbest enerjisi, σ_e, değerlerini hesaplamada kullanıldı. Yanal yüzey serbest enerjisi σ' nın bütün incelenen türler için değeri 10,4 erg/cm^2 olarak bulundu. Katlanma yüzeyi serbest enerjisi değerlerinin 15,5 erg/cm^2 ile 17,4 erg/cm^2 arasında değiştiği hesaplandı. Katlanma yüzeyi serbest enerjisi, σ_e, ile kristalleşme hızının moleküler ağırlığa bağlı olmadığı görüldü. Çekirdekleşme katkı maddeleri içeren türün kristalleşme hızının incelenen türler içinde en yüksek olduğu bulundu. Küresel yapıdan sapma olasılığının, daha küçük molekül ağırlıklı sınıflar için daha yüksek olduğu gözlendi.

Anahtar Kelimeler : polibüten-1, Lauritzen-Hoffman teorisi, yarıçapsal büyüme hızı, çekirdekleşme katkı maddesi, kristalleşme hızı, polimer kristalleşmesi

ACKNOWLEDGEMENT

I warmly thank Asst. Prof. Dr. Gurhan Kalay, for his great help and supervision throughout my studies.

TABLE OF CONTENTS

LIST OF FIGURES

LIST OF TABLES

LIST OF MOVIES INCLUDED IN THE APPPENDIX-1

A- Grade PB0110 Movies

1-011pb75c.avi
2-011pb80a.avi
3-011pb85a.avi
4-011pb85b.avi
5-011p90a2.avi

B-Grade PB0300 Movies

6-300pb55a.avi
7-300pb60a.avi
8-300pb65a.avi
9-300pb70a.avi
10-300pb75a.avi
11-300pb75c.avi
12-300pb80a.avi
13-300pb85a.avi
14-300pb90a.avi

C-Grade PB0400 Movies

15-400pb55a.avi
16-400pb60a.avi
17-400pb65a.avi
18-400pb70a.avi
19-400pb75a.avi
20-400pb75b.avi
21-400pb75c.avi
22-400pb80a.avi
23-400pb85a.avi
24-400pb90a.avi

D-Grade PB0800

25-800pb60a.avi

26-800pb65b.avi

27-800pb70a.avi

28-800pb75a.avi

29-800pb80a.avi

30-800pb85c.avi

CHAPTER-1. INTRODUCTION

Crystallization of polymers is important since their physical and chemical properties are dependent on the level of crystallinity. When a polymer melt is cooled to a temperature between a glass transition temperature and a crystal melting point, the crystallization of polymer takes place. Crystallization of polymers are kinetically controlled and affected by the crystallization temperature, thermal history of the polymer, pressure, shearing etc. Polymers show different structural features at different length scales. In the nanometer range, polymer chains form thin plate-like structures called lamella (of the thickness around 10nm). Since the thickness of lamellae is much less than the length of the polymer molecule, chains must be folded to form the lamellae. In the micrometer range, lamellae combine and result in a sphere-like structure called spherulite. Spherulites first appear as a small dot (nucleus) and grow with a constant speed. The number of spherulites affects the mechanical properties of the polymer. Spherulites are optically anisotropic structures and can be observed under the cross-polarized light.

The purpose of this study was to investigate the crystallization behaviour of different commercial grades of isotactic polybutene-1 and to design an experimental set-up for this investigation.

The mould temperature in processing could be chosen with such crystallization data in mind to obtain products exhibiting the desired mechanical properties. For instance the stiffness (Young's modulus) of the samples will be higher for smaller spherulite sizes than larger spherulite size samples. When toughness is important than the level of crystallization, should be kept lower by choosing the appropriate grade of polymer.

Isotactic polybutene-1 is quite an interesting polymer, i.e. it undergoes a crystal-crystal transformation upon ageing at room temperature. This crystal-crystal transformation is accompanied with the change of physical properties and development of cracks, which cause serious problems in the applications of the polymer. Therefore, polybutene-1 is not used in large quantities in comparison with the other lighter polyolefins like polyethylene and polypropylene, although isotactic

polybutene-1 has superior mechanical properties, i.e. tough, resistance to stress cracking, perfect resistance to creep even at elevated temperatures.

This thesis presents a literature review, in the next Chapter, i.e., Chapter-2. This chapter summarizes the synthesis, polymorphism, and crystal-crystal transformation of isotactic polybutene-1 and main features of the crystallization of polymers. This chapter includes a brief summary of the Lauritzen-Hoffman crystallization theory and its consequences. It also covers the previous work on the crystallization of polybutene-1 from literature.

The following chapter, Chapter-3, explains the set-up designed for this study and the methods used in crystallization calculations in Chapter-4, on the results and discussion. The experimental set-up designed for this study enables both fast cooling of the sample and record of the growth of spherulites as a real time movie. Then, the pictures can be obtained from this real time movies for further analysis.

The Chapter 4 gives the results of this study and these results are discussed on the basis of the previous literature work and Lauritzen-Hoffmann crystallization theory. The differences in the crystallization behaviour of the grades are discussed at the end of this chapter.

The final chapter summarizes the conclusions of this research together with some suggestions for a future study. A CD including the real time growth movies of the spherulites were also added as Appendix-1.

CHAPTER-2. POLYBUTENE-1 - LITEARATURE REVIEW

2.1 Introduction

Isotactic Polybutene-1 is a highly crystalline thermoplastic polymer with the crystal melting temperature (T_m) around 125 ^oC and the glass transition temperature (T_g) around –20 ^oC.[1] Polybutene-1 has several attractive mechanical properties; tough, resistant to stress cracking and abrasion and retains good mechanical properties even at high temperatures.[2] However, the commercial production of isotactic polybutene-1 is still small in comparison with polyethylene and polypropylene. The main reason has been the low level of monomer availability and its high price. In addition, crystalline transformation of processed articles at room temperature limits applications of iPB-1.[2]

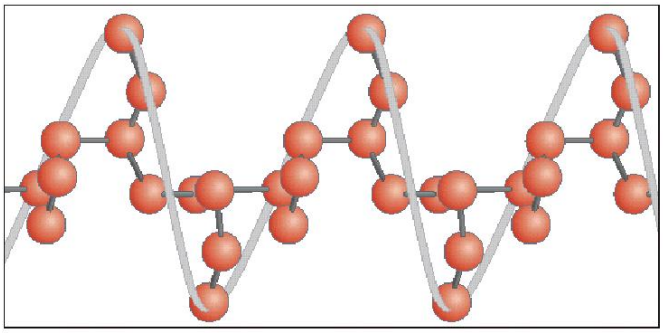

Figure 2.1 : Molecular Structure of Isotactic Polybutene-1[3]

2.2 Synthesis of Isotactic Polybutene-1

2.2.1Properties of Monomer

1-Butene ($H_2C=CHCH_2CH_3$) is a colourless flammable gas with boiling point of –6 ^0C at 1 atm.[4] Commercial production of 1-butene is either by the catalytic oligomerization of ethylene or by distillation MTBE (methyl tert-butyl ether) raffinate,[5] which is a high octane blending component for gasoline. Chevron, BP Amoco and Basell (formerly Shell) produce butene-1 by ethylene oligomerization. Exxon and Texas Petrochemicals distill butene-1 from other products during the production of MTBE.[2,5] More than half of the butene-1 produced is used as

polyethylene comonomer. Only 14 % of the total production in U.S.A. is used for the synthesis of polybutene-1.[5]

PRODUCER	CAPACITY*
BP Amoco, Pasadena, Tex.	120
Chevron, Cedar Bayou, Tex.	120
Exxon, Baytown, Tex.	140
Shell, Geismar, La.	140
Texas Petrochemicals, Houston, Tex.	315
Total	835

Table 2.1: Millions of pounds per year of butene-1 for chemical use, August 16, 1999[5]

2.2.2 Synthesis of iPB-1

Isotactic polybutene-1 is usually produced by solution polymerization of butene-1 with a Ziegler-Natta catalyst system.[6] (Solway or supported type catalyst) Cationic or free-radical initiators result in atactic PB-1 that do not crystallize.[4] The Synthesis of Isotactic polybutene-1 was first reported by Natta and co-workers in 1954.[2] Butene-1 polymerize readily with Ziegler-Natta catalysts to high molecular weight products.[7] In the early years, two component catalytic systems containing organoaluminium compounds with transition metal salt and halides were used.[2] A typical polymerization of butene-1 is as follows[7] : 0.049 mole $TiCl_4$ in 100 ml hexane is poured into a 10-litre dry flask filled with nitrogen and stirred while adding 0.049 mole $(Et)_3Al$ in 50 ml hexane. Butene-1 monomer is added at a rate of 40 litre/hour and the flask is stirred continuously. As necessary, hexane is added to decrease the viscosity. At the end, the reaction is quenched by ethyl alcohol. At room temperature, this reaction gives 160 gram of polybutene-1 in 3 hours. In addition to $TiCl_4$, chlorides of vanadium, molybdenum, tungsten and zirconium can be used in the preparation of catalysts. The metal can also be zinc or lithium instead of aluminium in the organometallic component and the alkyl group can be replaced by other alkyls such as phenyl, propyl, butyl.

A usual supported catalytic system is composed of a titanium halide, a Lewis base, anhydrous $MgCl_2$, an unsaturated intermediate, and a cocatalyst.[2]

Different stereospecific arrangements of PB-1 can be produced with a new kind of homogeneous Ziegler-Natta catalyst, which is composed of a group IVB metallocene and a methylaluminoxane (MAO).[2] The stereoregularity of the polybutene-1 can be controlled by the nature of the transition metal and the type of the ligand.[6] Stereorigid chiral ansa-metallocene catalysts with C_2 symmetry results in isotactic product (e.g. $Et_2(Ind)_2ZrCl_2$, $CH_2(Ind)_2Ti(CH_3)_2$). The products of these catalytic systems are highly isotactic and have narrow molecular weight distribution. In addition, the catalytic activities of these systems are very high.[2] The metallocenes with bilateral symmetry results in syndiotactic polybutene-1. (e.g. $Me(Cp)FluZrCl_2$, $CH_3CH(Cp)(Flu)ZrCl_2$).[6] Achiral and symmetric metallocenes generally results in atactic polybutene-1.[6] Stereoregular polybutene-1 can also be synthesized with half-titanocone/MAO, $Cp^*Ti(OBz)_3$/MAO.[6] Metallocene catalysts led to tailor made polyolefins with an efficient control of molecular weight distribution as well.

In addition to the butene-1, polybutene-1 can be synthesized also from butene-2.[2] 2-butene isomerises to butene-1 prior to propagation and the result of the reaction is polybutene-1.

2.3 Polymorpmism of Isotactic Polybutene-1

Isotactic polybutene-1 exhibits polymorphism in its crystalline structure.[2,9-35] Polymorphism of isotactic polybutene-1 have been studied mainly by DSC (differential scanning calorimetry), XRD (X-ray diffractometry), FT-IR (fourier transform far infrared spectroscopy), TEM (transmission electron microscopy), AFM (atomic force microscopy), dilatometry, electron crystallography and Raman spectroscopy. Five different crystalline structures of isotactic polybutene-1 have been determined: Form-I, Form-II and Form-III, Form-I' and Form-II'. They have different packing of chains leading to different unit cell geometries, sizes and symmetries. Thus, their physical properties like density, melting point, mechanical properties are also different.

Crystallization of melt at room temperature produces metastable Form-II. Form-II, then, gradually transforms into the stable Form-I at room temperature[2] Form-I is characterized by a trigonal (hexagonal) unit cell with dimensions a=b =1.77 nm

and c(chain axis)=0.65 nm.[9] Space group of the unit cell of Form-I is R3c or $R\bar{3}c$ with 3/1 helical conformation of the chains (twinned). The melting point of Form-I is around 130 ^{o}C at atmospheric pressure. AFM studies has shown that Form-I of iPB-1 is also stable on the surface of the polymer as well as in the bulk.[21]

Form-II of isotactic polybutene-1 can be directly obtained by crystallization from melt at atmospheric pressure, from dilute solutions of certain solvents at certain temperatures,[15,16,24,] with annealing of Form-III and Form-I' at certain temperatures[24] and also by epitaxial crystallization.[17] Crystallization on a substrate surface from the bulk is called epitaxial crystallization. Form-II is characterized by tetragonal unit cell with dimensions a=1.542 nm, b=2.105.[12] Molecular chains with 11/3 helical conformations are packed to give $P\bar{4}$ space group. Melting point of Form-II is around 118 ^{o}C at atmospheric pressure. Figure 2.2 shows schematically the helical conformations of Form-I and Form-II.

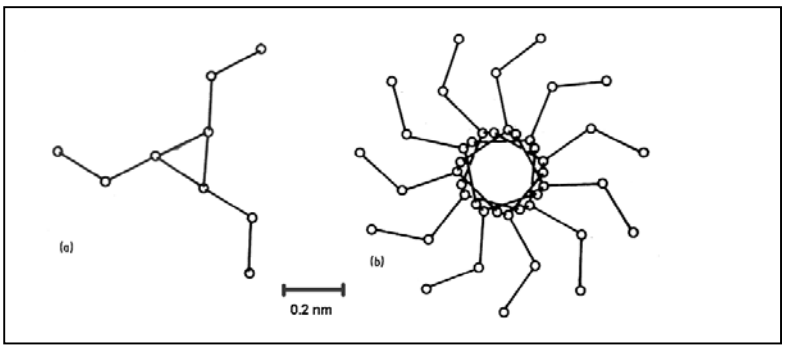

Figure 2.2 : Helical conformations of (a)Form-I, 3/1 helix (b)Form-II, 11/3 helix[39]

Form-III of isotactic polybutene-1 can be obtained by crystallization from dilute solutions of certain solvents at certain temperatures,[15,16,19,24] by epitaxial crystallization[17,19] and by polymerization at high temperatures up to 100 ^{o}C.[2] Form-III is characterized by an orthorhombic unit cell with dimensions a=1.238, b=0.888, c(chain axis)=0.756nm.[19] Molecular chains with 4/1 helical conformation are packed to give a $P2_12_12_1$ space group. Form-III has a melting point around 95 ^{o}C at atmospheric pressure. Form-III is stable at room temperature but unstable at temperatures near its melting point. The annealing temperature determines whether the transformation would be into Form-II or Form-I'.[24]. Figures 2.3 and 2.4 shows DSC thermograms and X-ray diffraction patterns of various polymorphs of iPB-1, respectively.

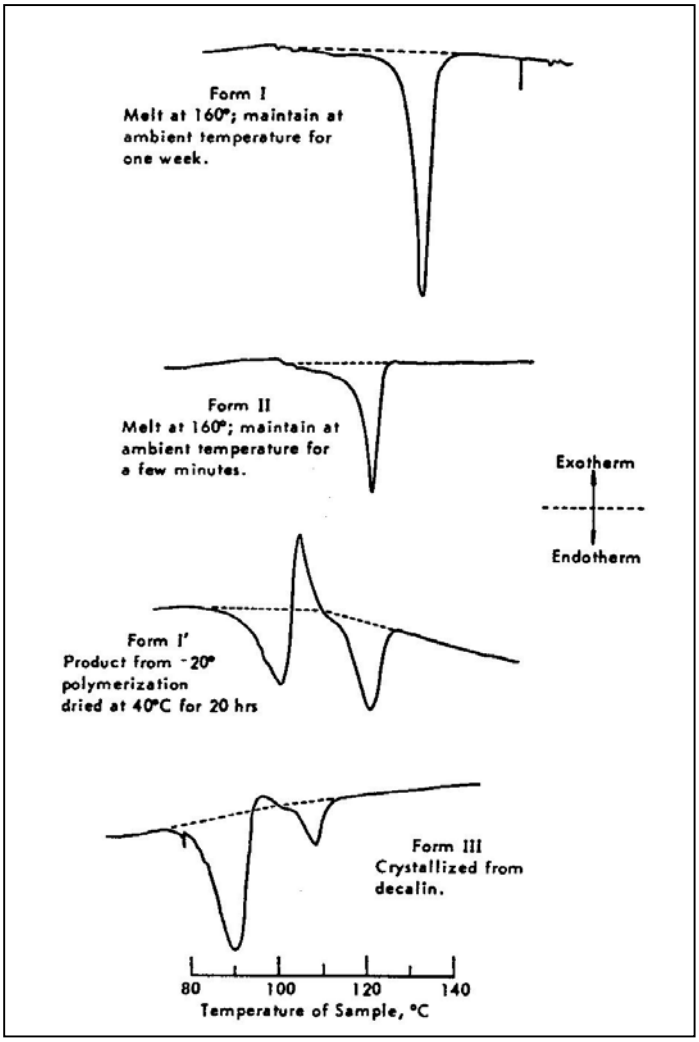

Figure 2.3: DSC thermograms of various polymorphs of iPB-1[11]

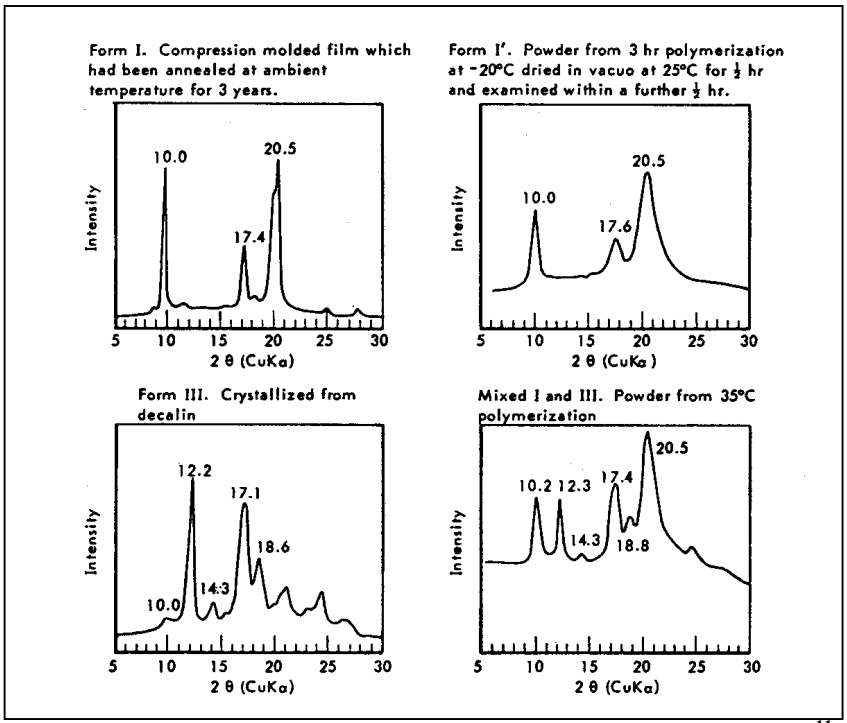

Figure 2.4 : X-ray diffraction patterns of various polymorps of iPB-1[11]

Form-I' of iPB-1 can be obtained by melt crystallization under high pressure[13] or if shear is applied to a solidifying melt[34], by crystallization from certain solvents at certain degrees[24] and by epitaxial crystallization.[18,20] Form-I' can also be obtained by polymerization at low temperatures.[11] Form-I' is stable at room temperature but transforms into Form-II upon annealing near its melting point. Form-I' has the same unit cell as Form-I except that molecular chains are untwinned. The Form-I' has a melting point around 95 ^{o}C at atmospheric pressure. [2]

The fifth polymorph, Form-II' can only be obtained by crystallization under high pressure. Form-II' is not stable and transforms into Form-I' at room temperature and atmospheric pressure. [13]

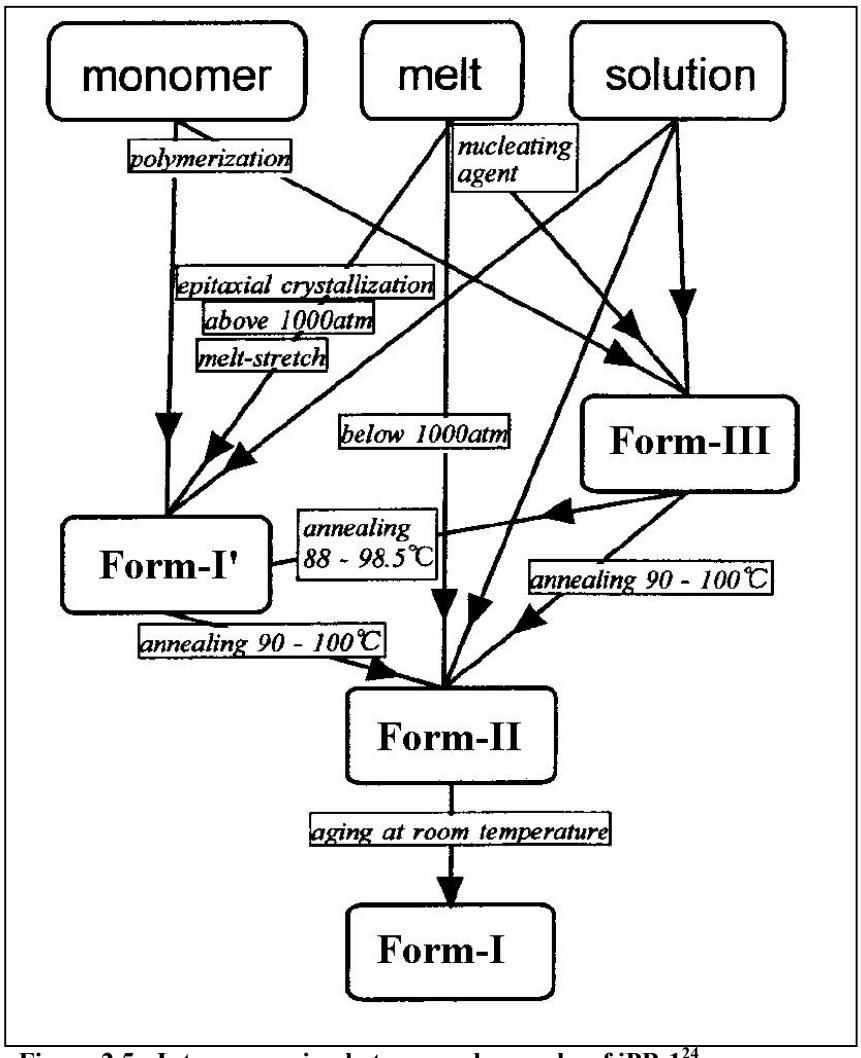

Figure 2.5 : Interconversion between polymorphs of iPB-1[24]

2.4 Form-II to Form-I Crystal Transformation

2.4.1 Introduction

The figure 2.5 above summarizes the various crystal-crystal transformations of iPB-1.[24] For the crystallization from solution, only an amyl acetate solution is considered for simplicity. The most important of these is the crystal transformation of Form-II into Form-I upon standing at room temperature and atmospheric pressure. This transformation is a solid state transformation. This transformation is heavily studied because of its commercial importance. Form-II spontaneously transforms into the more stable crystalline structure Form-I.[2,23-30,32,33] In other words, moulded articles have Form-II crystal structure just after the moulding process. This crystal transformation is accompanied with the change of physical properties; increase of melting point, heat of fusion and density. However, the shape of the moulded objects does not change considerably. This transformation may cause crack formation.[23] Cracks develop in the structure since the density increases. These cracks affect mechanical properties adversely. Figure 2.6 illustrates the development of cracks during this transformation. This transformation results in a increase in the length of a molecule of about 14% and a decrease in cross-section area of about 10%. [2]

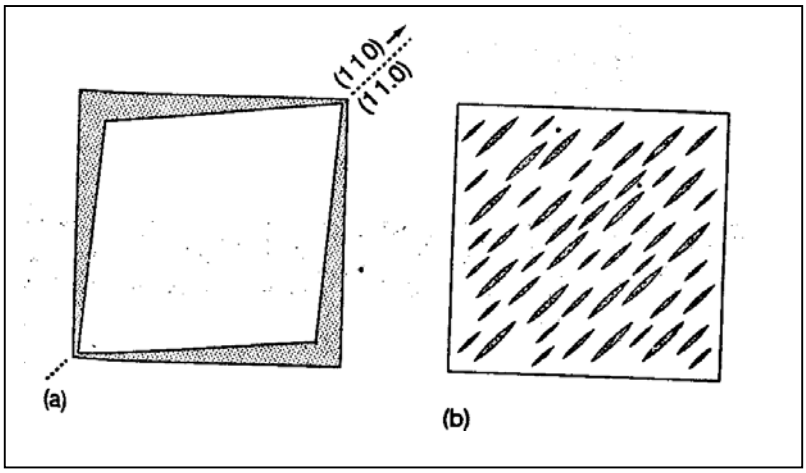

Figure 2.6 : (a)Shrinkage(shaded area) of square Form-II crystal upon conversion to Form-I when the indicated $(110)_I$-$(11.0)_{II}$ plane is maintained in the transformation (b)Development of cracks and elongated domains to accommodate this shrinkage when the overall crystal dimensions are constrained[23]

The application of macroscopic shears during processing as in the case of shear controlled orientation injection moulding (SCORIM) results in mouldings with completed Form-II to Form-I transformation. Therefore the development of possible crack formation at room temperature could be avoided.[34,52]

2.4.2 The Rate of Transformation From Form-II to Form-I

This transformation may take days to weeks depending on the conditions.[23] Form-II completely transforms into Form-I in one week at room temperature and atmospheric pressure. The rate of this transition is affected by thermal history, temperature, mechanical deformation, pressure, orientation, x-ray radiation, molecular weight and tacticity, additives, blends, nucleating agents, and copolymerization. [2]

The transformation of Form-II into Form-I is through a nucleation processs and follows the Avrami equation where $V_x(t)$ is the volume fraction of the the Form-I (transformed). [14,28,32]

$$V_x(t) = 1 - \exp (- Kt^n). \qquad \text{Eq. 2.1}$$

Here K is the rate constant and n is Avrami constant which depends on both form of nucleation and growth of the stable phase.

Figure 2.7 shows the overall conversion of Form-II to Form-I as a function of time for three different take up speed for iPB-1 fibers. Avrami type fits are shown in Figure 2.7 as solid lines. The change of overall crystallinity with time clearly fits to Avrami equation. As the take up speed is increased, orientation of molecular chains in the iPB-1 fibres increase. And as the molecular orientation increases, the rate of transformation from Form-II to Form-I increases. This is akin to what is observed for SCORIM moulded iPB-1as mentioned above.

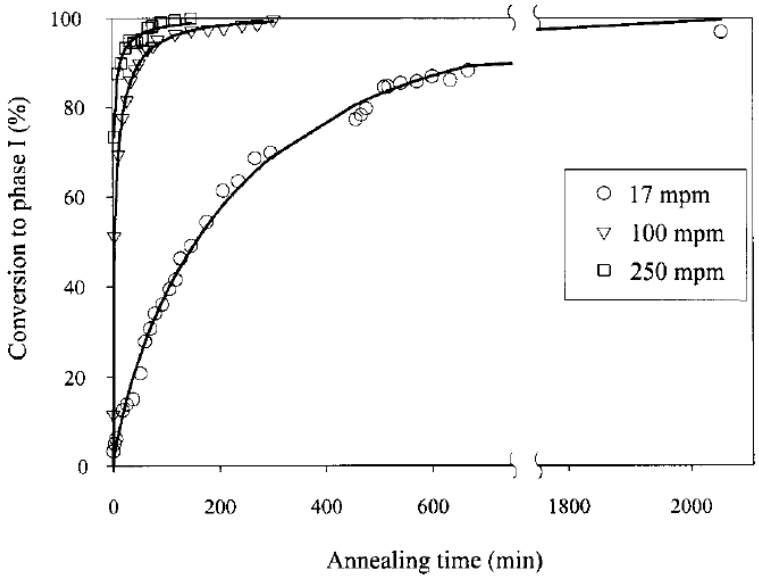

Figure 2.7 : Percentage conversion to stable Form-I as a function of annealing time for different take up speeds. Avrami-type fits to data are shown as solid lines on the graph.[32]

This transformation is fastest at room temperature. The rate of transformation decreases as the temperature is increased or decreased. No transformation is observed at 100 ^{o}C or at dry ice temperatures.[2,29] The transformation can be completed in a few seconds under hydrostatic pressures above 100 atm. The uniaxial stretching of the polymer also increases the rate of transformation sharply. It is considered that uniaxial stretching helps molecules to rearrange since transformation is accompanied with a decrease in the cross-section and an increase in the length of the molecule. The application of external stresses also increases the rate of transformation through increasing the rate of nucleation.[2] The rate of the transformation is also affected by the thickness of the films. [25] In the absence of external stress, the rate of transformation decreases with decreasing film thickness. However, when external stresses are applied the relation is reverse. As the film thickness is decreased, the rate of transformation increases. In a study on the crystal growth rate of poly(ethylene oxide), a remarkable slowing down of the crystal growth for films with thicknesses less than approximately 100 nm was observed.[54] For the poly(ethylene oxide) films with thicknesses over 200 nm, no change in the spherulite growth rate is observed.

The rate of transformation can easily be followed by FT-IR spectroscopy.[29] Form-II and Form-I have completely different spectra from 1500 to 450 cm^{-1}. Figure 2.8 shows the FT-IR spectra of films of iPB-1 aged at room temperature for various

times. The sample aged for 15 minutes and the one aged for 1 year correspond to unstable Form-II and stable Form-I, respectively. The bands at 905 cm^{-1} and 924 cm^{-1} allow us to differentiate between these two forms of iPB-1. The one at 905 cm^{-1} is the characteristic band of Form-II and the one at 924 cm^{-1} is the characteristic band of Form-I.[25] The half-life of this transformation can be determined with the ratio of IR extinction of these two peaks. Half-time is reached when the ratio of IR extinction of Form-I (924 cm^{-1}) to IR extinction of Form-II (905 cm^{-1}) equals approximately 1.5

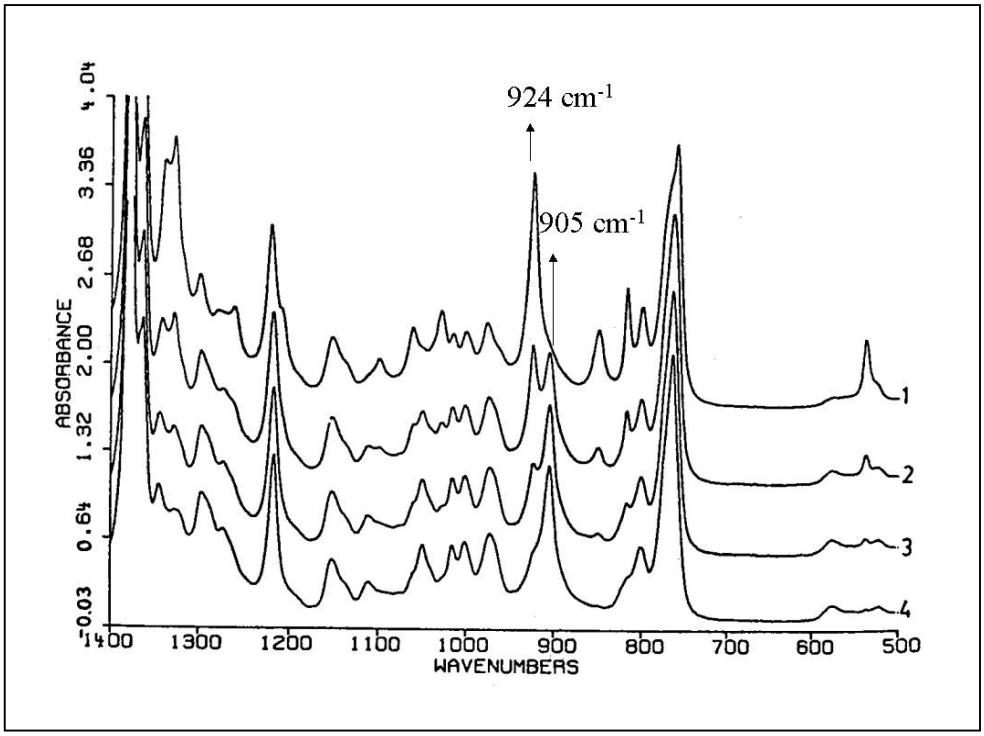

Figure 2.8 : IR spectra of iPB-1, curve 1 = aged for 1 year, curve 2 = aged for 10 h, curve 3 = aged for 2 h, curve 4 = aged for 15 min[25]

2.5 Polymer Crystalllization

2.5.1 Introduction

A crystal has lower free energy than liquid at temperatures below the thermodynamic melting point T_m^o. [40] Figure 2.9 shows the change of thermodynamic variables at T_m^o. The crystallization of polymers is associated with a negative Gibbs free energy. However, the arrangement of all chains requires a large negative entropy of activation. Below the glass transition temperature T_g, the energy of the chains is not enough to rearrange and this restricts the crystallization between T_g and T_m.[37] It can be said that the crystallisation of polymers is kinetically rather than thermodynamically controlled. Polymers do not crystallize completely unlike oligomers.[37] Entanglements of the chains prevents the formation of complete crystalline order. The exact nature of the polymer crystals is not known completely yet although there are a few models to explain the crystal structures of polymers.[40]

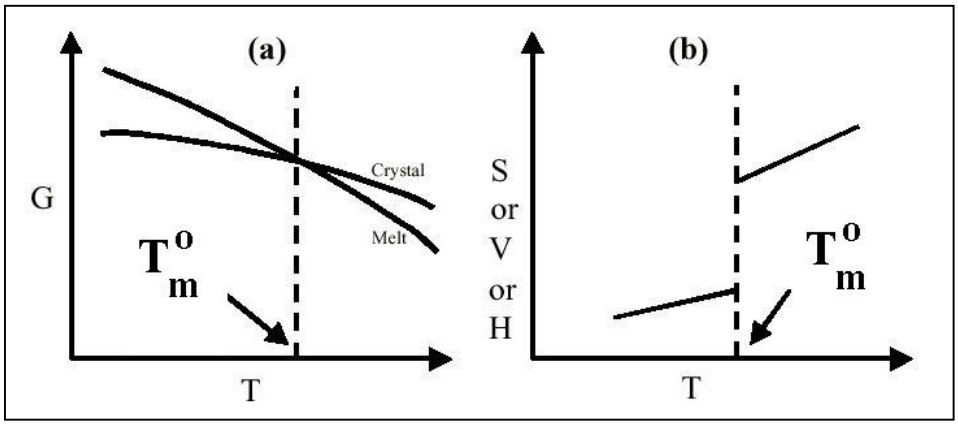

Figure 2.9 : General Behaviour of thermodynamic variables at the equilibrium melting temperature T_m^∞ (a)Gibbs free energy (b) Entropy, Volume and Enthalpy [40]

The first step of the crystallization is the formation of a stable nucleus. (nucleation). Nucleus is formed by the parallel ordering of the chains stimulated first by intramolecular forces and then stabilised by the secondary valence forces (long range order forces), which provides the packing of molecules into a three-dimensional ordered structure.[37]

Nucleation is followed by the growth of the crystal region. The size of the crystal increases as the new chains added to the crystalline region. Thermal

redispersion of the chains at the crystal-melt interface counteracts the growth of the crystal.[37]

The extended chain morphology, in which all the chains are parallel and the size of crystal equals the extended length of a chain, is considered as the equilibrium morphology for most polymers.[36] However, the exact morphology of the polymer crystals depends on the crystallization conditions. We can classify the crystallization of polymers under three main groups: [36,40]

I-Crystallization during polymerization

II-Strain induced crystallization

A-crystallization from solutions under strain

B-crystallization from melts under strain

III-Crystallization under quiescent condition

A-crystallization from quiescent solutions

B-crystallization from quiescent melts

2.5.2 Crystallization during polymerization[40]

The crystal obtained during polymerization is not just a consequence of the change in physical state. The crystal is obtained during chemical reactions at the gas/solid or the solid/liquid interfaces. The mechanism of crystallization might be simultaneous polymerization and crystallization, or crystallization follows the polymerization. Macroscopic crystals can be obtained by crystallization during polymerization. The crystalline structure of the polymer is also affected by the polymerization conditions.[13]

2.5.3 Strain Induced Crystallization

2.5.3.1 Crystallisation from Solutions under Strain

When there is no external force, there is no preferred orientation of polymer chains (unoriented). However, if an external force is applied, the polymer chains are oriented and this orientation of chains ends up with a different crystal morphology.[36] When a dilute polymer solution (1 %) is stirred during crystallization, shish-kebabs may form. The backbone, shish, is composed of extended chains and kebabs grow epitaxially on this backbone.[36]

2.5.3.2 Crystallisation from Melts under Strain

Similar to the solution case, the applied force results in the orientation of polymers. By the application of shear to a solidifying melt, shish-kebabs can be formed. The mechanical properties of the articles can be improved by the formation of shish-kebab morphology.[34] Figure 2.10 shows the AFM image of a SCORIM moulded polybutene-1. The interlocking shish-kebabs can be clearly seen in this image.

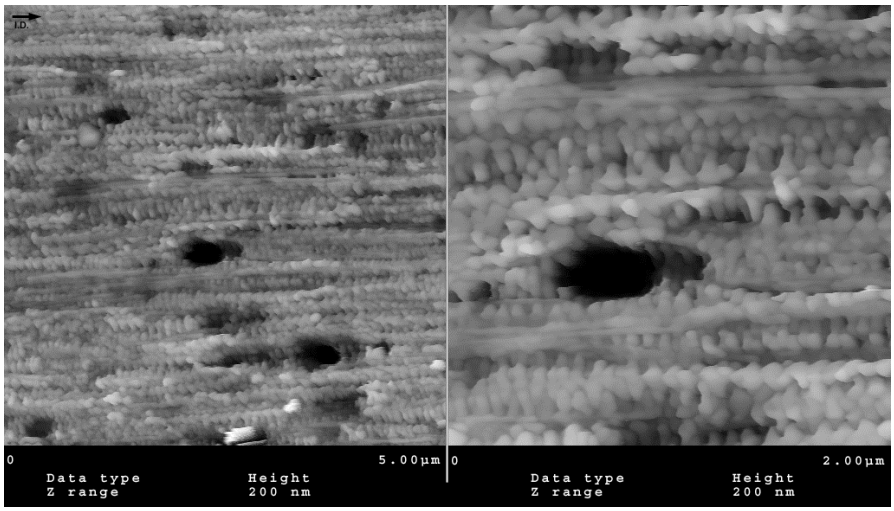

Figure 2.10 :AFM image of the shear region of iPB-1 processes by SCORIM. The injection direction is identified with an arrow[34]

Application of stress to an amorphous or a semi-crystalline polymer between T_m and T_g is likely to increase the crystallinity of polymers since the polymer chains

are oriented in the direction of applied stress. The process known as cold-drawing is done between this temperature range.

2.5.4 Crystallisation under Quiescent Condition

2.5.4.1 Crystallisation from Quiescent Solutions

A single crystal of polymers from solution was first reported in 1953. Before, it was believed that single crystals could not be produced from solutions because of molecular entanglements. Later, single crystals of so many polymers obtained from their solutions. The single crystal of polyethylene in shown in Figure 2.11. Pleats in the crystal may occur often.[36]

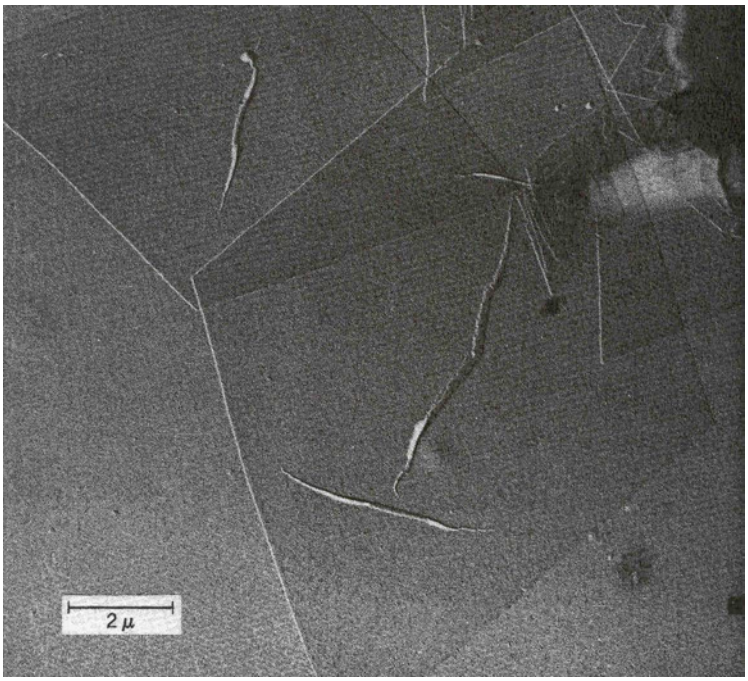

Figure 2.11 :Electron micrograph of linear polyethylene grown from a solution of perchloroethylene[36]

The single crystals of all polymers have the same geometry, thin and flat platelets. The thickness of these platelike structures is around 10 nm and the lateral dimensions may go up to micrometers. These platelike single crystals are called **'lamella'**. The thickness of the single crystals may increase by the formation of new lamellae on the screw dislocation of the preformed lamellae. The geometry, size and

regularity of the crystals are determined by the crystallization conditions like temperature and solvent type.[36]

The electron diffraction measurements demonstrated that that polymer chains are aligned normal or nearly normal to the plane of the lamellae. Since the length of a polymer molecule is generally much larger than the thickness of the lamellae, it can be concluded that the chains are folded during the formation of lamellae. Different models have been proposed to explain the nature of the folding surface as shown in Figure 2.12[36]

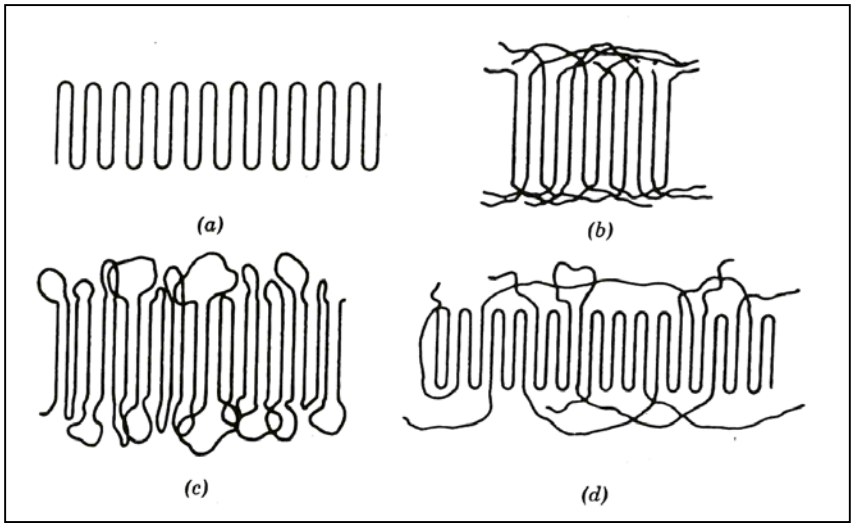

Figure 2.12 : Schematic two dimensional representations of models of the the fold surface (a)sharp folds (b) "switchboard" model, (c) loose loops with adjacent reentry (d) a combination of several features.[36]

The structural and kinetic evidences show both there is a regular folding of chains with immediate reentry into the crystal and also a considerable molecular disorder exists in polymer single crystals. The extent of the disorder is too large that it can not be considered as a result of intercrystalline defects and implies existence of some amorphous region at the fold surface. The "switchboard" and "adjacent entry with loose loops" models have been suggested to explain the existence of the amorphous region.[36]

In addition to lamellae, the crystallization from the solution may result in complex structures similar to those found in polymers crystallized from the melt.

Formation of sheaflike arrays similar to spherulites, dendritic growths, clusters of hollow pyramids, spiral growths, dislocation networks are also reported.[36]

2.5.4.2 Crystallization from Quiescent Melts

2.5.4.2.1 Fringed Micelle Model

Bragg reflections of polymers are broad and diffuse unlike that of the well-developed single crystals. This broadening is assumed to be the result of small crystallite size but not because of the imperfections of the crystal. Therefore, the size of these crystals is in the order of the 10 nm, when calculated considering the broadening of the lattice. Since the chains are much longer than this distance, the fringed micelle model has been suggested which states that chains contributes to several crystalline and amorphous regions.[36]

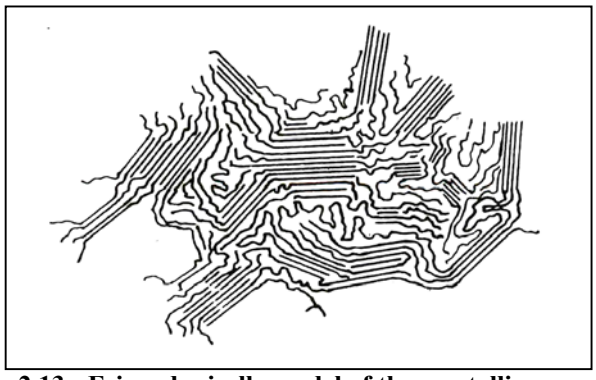

Figure 2.13 : Fringed micelle model of the crystalline-amorphous structure of polymers[36]

The fringed micelle model is quite simple and successful for the explanation of good mechanical properties as a result of combined crystal and amorphous layers and simple interpretation of degree of crystallinity. However this model can not explain the growth of spherically symmetrical structures called spherulites. This was overcome by the later discovery of polymer single crystals with lamellar structures including chain folding. Spherulites are shown to be complex structures of lamellae. Therefore it was concluded that the fringed micelle model is inaccurate for the general crystallization of polymer from quiescent melts.[36] However the fringed micelle model is not absolutely obsolete and still can be used in order to explain some phenomena

occurring in the crystallization of polymers like gelation during polymerization and crystallization during rapid cooling/quenching.[40]

2.5.4.2.2 Spherulites

Spherulites are spherical aggregates of lamellae's with sizes ranging from submicroscopic sizes to milimeters.[39] Spherulites are observed as circular birefringent areas possessing a dark Maltese cross pattern. A schematic of Maltese cross pattern and a spherulite of iPB-1 are shown in Figure 2.14. The orientation of Maltese cross depends on the direction of polarizer and analyser. As the polarizer are rotated, the maltese cross also rotates.

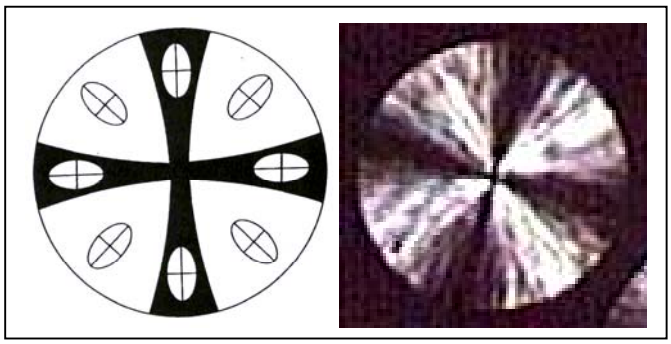

Figure 2.14 : A schematic diagram of ordering of the indicatrices in a spherulite and the resulting Maltese cross extinction pattern and a micrograph of spherulite of iPB-1.[39] The single spherulite on the right is taken from the real time movies of spherulitic growth investigated in this thesis.

A schematic of structure of a spherulite is shown in Figure 2.15. The spherulites consists of fibrils and fibrils consists of lamellae radiating outward.[37] The chain folding direction is transverse to the radial direction.[39] Between the lamellae there exist amorphous regions and tie chains that connects the lamellae.[37]

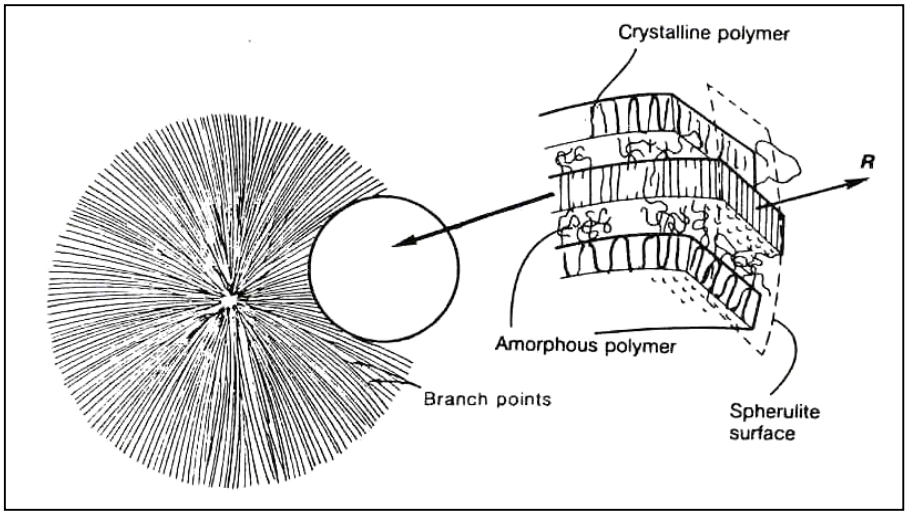

Figure 2.15 : A Schematic diagram of fully developed spherulite grown from the melt.[37]

In Figure 2.16, the right side is the electron micrograph of a spherulite of iPS at an early stage of development. The central part is composed of parallel layers. As the spherulite grows, these layers become curved and at the end the sphere forms. Splaying and branching are necessary since the surface area increases as the spherulite grows.[39]

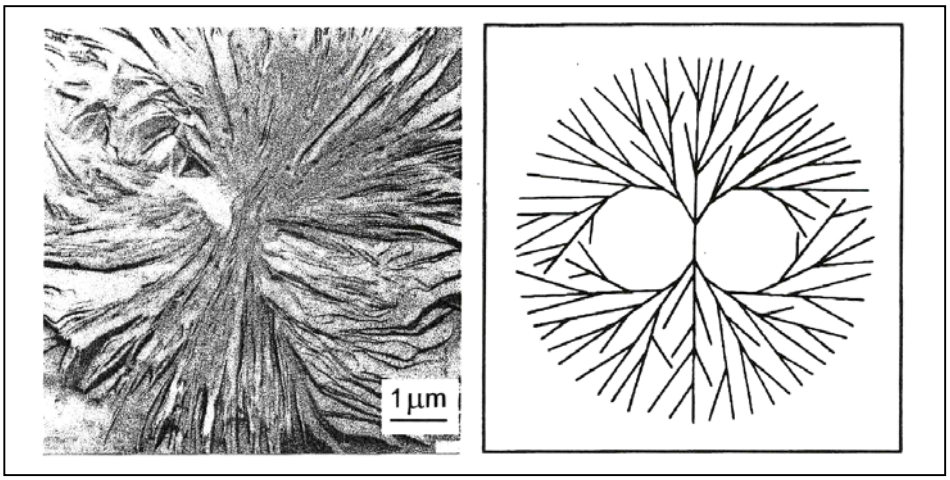

Figure 2.16 : Left :Electron micrograph of central sheaf-like part observed at an early stage of development of a spherulite of iPS. Right : schematic of branching and splaying in the fully developed spherulite[39]

If the refractive index along the transverse direction is greater than that of along the radial direction, spherulite is called as negatively birefringent and when the refractive index along the radial direction is bigger than that of the transverse direction, spherulite is called as positively birefringent.[37] Spherulites also might have zigzag patterns, concentric rings (ringed spherulites), and dendritic structures.[37]

2.5.4.2.3 Nucleation

There are two main groups of nucleation : heterogeneous and homogeneous. Heterogeneous nucleation is due to foreign particles. These foreign particles (or surfaces) must reduce the boundary surface energy, must have a melting point above that of the polymer and must be insoluble in the polymer melt.[38] Nucleating agents increase the nucleation rate but does not influence the spherulitic growth rate.[37]

Homogeneous nucleation is the nucleation of the polymer without a second surface or pre-existing nuclei. Homogeneous nucleation can be thermal or athermal. If the random fluctuations of chains result in crystal-like regions (embryos), these are called thermal nucleus.[38] These embryos are not stable above the melting point and no crystallization begins. Below the melting point, the critical size of the nucleus depends on the temperature. This is shown in Figure 2.17. As the temperature increases, the critical size of the nucleus also increases. Above this critical size, the formation of nucleus is favoured. Below this size, the embryo is not stable and no nucleation takes place. [38]

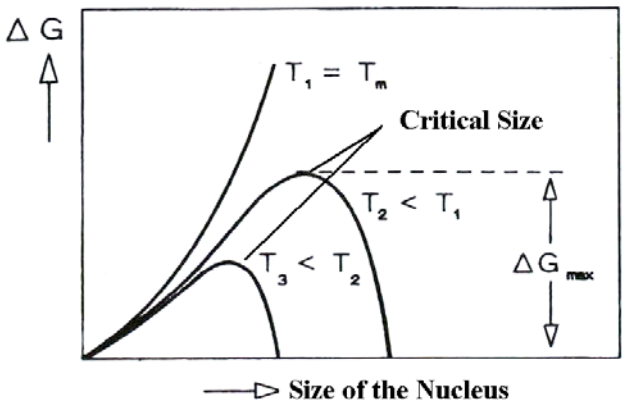

Figure 2.17 : Free energy of crystal nuclei formation as a function of temperature.[38]

The following equation describes the rate of thermal nucleus formation where $\eta(T)$ is the viscosity of material at temperature T, ΔG_{max} is the activation energy for nucleus formation and N_o is normalization factor:[38]

$$\dot{N} = \dot{N}_o \frac{T}{\eta(T)} e^{\Delta G_{max}/RT} \qquad \text{Eq. 2.2}$$

The thermal nucleation rate increases as the temperature decreases since ΔG_{max} decreases. As the temperature decreases more, the rate of thermal nucleation first goes through a maximum and then decreases as the temperature gets close to T_g. The change of primary and secondary nucleus formation rates as a function of crystallization temperature is shown in Figure 2.18 As the temperature decreases, the changes in the viscosity term, $T/\eta(T)$, is responsible for the decrease of the nucleation rate.[38] As the viscosity increases, the possibility of chains to form primary nucleus through random molecular motion of chains decreases since the kinetic energy of the chains decreases.[37]

The molecular weight of the polymer affects the nucleation rate through the viscosity of the polymer melt.[37] As the molecular weight of the polymer increased, the viscosity increases and final result is the decrease of the rate of thermal nucleation.

As for the athermal nucleation, when the temperature falls rapidly, a crystal embryo becomes stable nucleus since the critical size decreases as the temperature is decreased. Therefore, with a rapid drop in temperature, the athermal nucleations take place at the same time and this give rise to the same spherulite size whereas thermal nuclei result in different sized spherulites since nucleation takes place at different times.

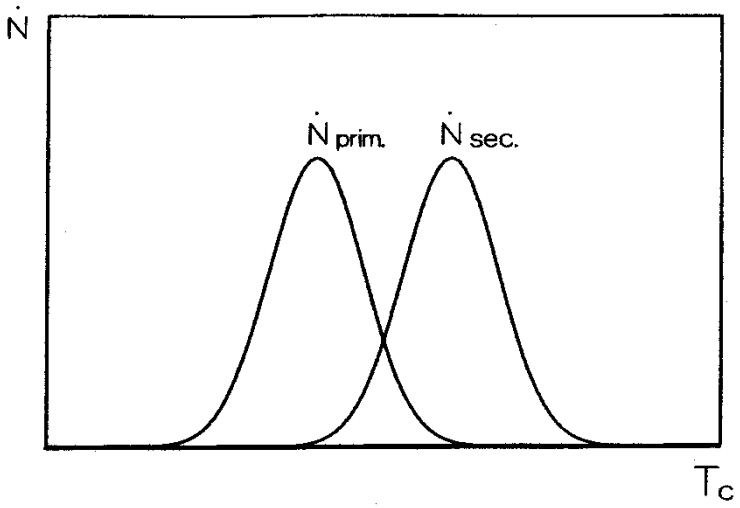

Figure 2.18: Primary and secondary nucleus formation rates as a function of crystallisation temperature.[38]

2.5.5 Kinetics of Lateral Crystal Growth

The growth of the crystal occurs by secondary and tertiary nucleations on the crystal surface.[38] The activation energy of secondary and tertiary nucleations is smaller than the primary nucleation.[38] This is due to the new interfacial area formed as a result of growth. The interfacial area decreases as the order of nucleation increases. Therefore, the maximum of the secondary nucleation rate is at higher temperatures than the maximum of the primary nucleation rate as shown in Figure 2.18. As a result, the size and number of the crystals formed depends on the crystallization temperature T_c. Provided that a constant degree of crystallization, at low temperatures a high number of small crystals form. Whereas at high temperatures, a small number of big crystals forms. [38]

2.5.5.1 Lauritzen-Hoffman Secondary Nucleation Theory

Lauritzen-Hoffmann secondary nucleation theory explains the crystallization kinetics (effect of temperature on crystal growth rate) of linear flexible polymers which are crystallized from melt into a lamellae by chain folding. The theory is also applied for the crystallization kinetic of more rigid polymer like PEEK.[40]

The theory accounts for a wide range of experimental observations like the variation of lamellar thickness by degree of supercooling, break in temperature dependence of growth rate, the origin of σ and σ_e (respectively lateral surface interfacial free energy and fold surface interfacial free energy), the effect of adjacent (tight folding) and non-adjacent events (tie chains, loose folds, cilia). However, the theory can not address completely the primary nucleation (thus the bulk crystallization kinetics), how a lamellae develops from a primary nucleus, how the lamellar branching give rise to spherulites, banding in spherulites, and quantified estimation of degree of crystallinity.[36,40]

Preliminary assumption of the theory is chain folding. The lamellar formation is kinetically controlled and results in a metastable crystal. The thermodynamically stable form is extended chain crystal. Increase of the melting point upon extended annealing shows that formed lamellae is not yet a stable product.[41] The treatment in

the theory starts with the deposition of first stem and later stepwise deposition of subsequent stems are considered.[40] A stem is the portion of chain occupying the length l_g^*, the fold thickness of lamella. (see Figure 2.19).

The rate constants for the deposition of the first step, where A_o is for forward and B_1 is backward reaction rates :[40,44,8]

$$A_o = \beta \exp\left(\frac{-2b_o l\sigma + \phi a_o b_o l \Delta G_f}{kT_c}\right) \qquad \text{Eq. 2.3}$$

$$B_1 = \beta \exp\left(\frac{-(1-\phi) a_o b_o l \Delta G_f}{kT_c}\right), \qquad \text{Eq. 2.4}$$

where β : retardation factor related to the transport machanism of the chain to the nucleation site,

σ : lateral surface interfacial free energy,

σ_e : fold surface interfacial free energy,

a_o : width of the crystalline stem,

b_o : thickness of the crystalline stem,

l : length of the crystalline stem,

ΔG_f : free energy per unit volume,

Φ : Fraction of ΔG_f apportioned to the forward reaction.

k : Boltzmann constant

and for the subsequent steps the rate constants for the forward and backward reaction are :[40,44]

$$A = \beta \exp\left(\frac{-2b_o l\sigma_e + \phi a_o b_o l \Delta G_f}{kT_c}\right) \qquad \text{Eq. 2.5}$$

$$B = B_1 \qquad \text{Eq. 2.6}$$

From the steady state flux calculations, the rate of stem deposition can be expressed as :[40,44]

$$S(l) = \frac{N_o A_o (A - B)}{A - B + B_1} \qquad \text{Eq. 2.7}$$

where N_o is the number of initial stems which can crystallize and in front of the substrate.

The parameters leading up to crystal growth rate 'G' are the surface nucleation rate i and substrate completion rate g. The rate of stem deposition equals :[40,44]

$$i = \frac{l}{n_l a_0 l_u} \int_{2\sigma_e/\Delta G_f}^{\infty} S(l)dl \,, \qquad \text{Eq. 2.8}$$

where n_l is the number of stems with length a_o in a substrate length L ($n_l a_o = L$) and l_u is the monomer length (projected length per monomer unit). Then,[40,44]

$$i = \frac{N_o B}{n_l a_o l_u}\left[\frac{kT_c}{2b_o\sigma} - \frac{kT_c}{2b_o\sigma + \Delta G_f}\right]\exp\left[\frac{-4b_o\sigma_e\sigma}{\Delta G_f kT_c}\right] \qquad \text{Eq. 2.9}$$

and the rate of substrate completion equals $g = a_o(A - B)$. Then,

$$g = a_o\beta \exp\left(\frac{N_o B}{n_l a_o l_u}\right)\left[\exp\left(-\frac{2a_o b_o\sigma_e}{kT_c}\right) - \exp\left(\frac{-a_o b_o l\Delta G_f}{kT_c}\right)\right] \qquad \text{Eq. 2.10}$$

The nature of the relation of G on i and g depends on the relative rates of i and g. These are shown in Figure 2.19 [40] The rate of crystal growth G corresponding to different regimes of growth can be calculated from the Figure 2.19 and results are shown in the Figure 2.19 as well.

The retardation factor β, which is related to the transport mechanism of the chain to the nucleation site, can be described as :[40]

$$\beta = J\exp\left[\frac{-U^*}{R(T - T_\infty)}\right] \qquad \text{Eq. 2.11}$$

where U^* is the activation energy for chain transfer, T_∞ is the temperature at which all motion associated with viscous flow stops and the polymer is like a solid, R is gas

constant and *J* is a factor, which is given as below in a recent version of the L-H crystallization theory :[40]

$$J = \frac{\kappa}{n}\left(\frac{kT}{h}\right) \qquad \text{Eq. 2.12}$$

where *h* is Planck's constant, κ is a numerical constant evaluated from the monomeric friction constant and the '$\frac{kT}{h}$' is a frequency factor in events per second and *n* is the number of repeat units.

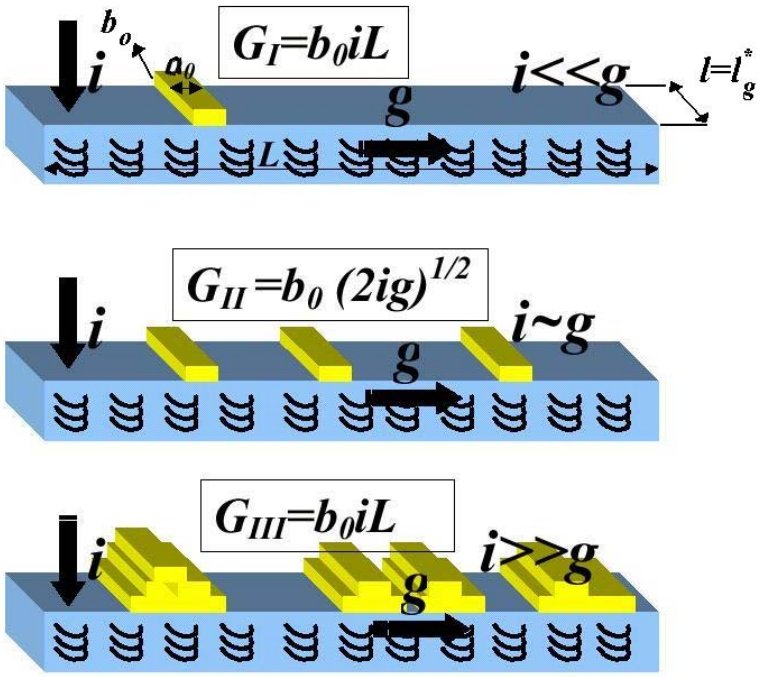

Figure 2.19 : Scheme illustrating the rates of stem deposition during three different regimes of crystallization, 'i' represents the rate of stem nucleation whereas 'g' represents the rate of substrate completion[40]

When we substitute these relations for the '*i*' and '*g*' in the equations for the growth rate *G* for different regimes as shown in Figure 2.19, the growth rate G for these regimes equals :[40]

$$G_I = G_{0I}\exp(-U^*/R(T-T_\infty))\exp(-K_{gI}/T\Delta T_c) \qquad \text{Eq. 2.13}$$

$$G_{II} = G_{0II}\exp(-U^*/R(T-T_\infty))\exp(-K_{gII}/T\Delta T_c) \qquad \text{Eq. 2.14}$$

$$G_{III} = G_{0III}\exp(-U^*/R(T-T_\infty))\exp(-K_{gIII}/T\Delta T_c) \qquad \text{Eq. 2.15}$$

Where,

$$G_{0i} = \frac{N_0 b_0 J}{l_u}\left[\frac{kT}{b_0\sigma} - \frac{kT}{2b_0\sigma + a_o b_0 \Delta G_f}\right] \qquad \text{Eq. 2.16}$$

and $K_{gI} = K_{gIII} = 2K_{gII} = \frac{4b_0\sigma\sigma_e T_m^o}{k\Delta H_f}$ Eq. 2.17

2.5.5.2 Regimes of Growth

In Regime –I, the rate of substrate completion is much bigger than the rate of stem nucleation and no new nucleus forms before the first layer is completely filled.[40] Many molecules may be necessary to complete the layer. In this regime, adjacent reentry of molecules takes place and deposition rate is highly affected by the temperature.[41]

In Regime-II, the rates substrate completion and stem deposition has the same order and new nuclei can form before the previous layer is completely filled. Larger undercooling is necessary to reach Regime-II in comparison with the Regime-I. Also in this regime, adjacent reentry of the molecules is assumed.[40,41]

In Regime-III, the rate of stem nucleation is much bigger than the rate of substrate completion and as a result the high number of nuclei form on the existing layers before the completion of the layer. The crystallization rate is very high and supercooling is higher than those of Regime-I and Regime-II. In this regime, chains do not undergo adjacent reentry. The chains fold via a type of 'switchboard model' and they have only a few folds before entering the amorphous phase and free to reenter the same lamellae.[40,41]

2.5.5.3 Spherulite Growth Rate vs Temperature

The radial growth of spherulite is usually linear at constant temperature.[41] The growth rate of spherulites approaches zero at T_m and T_g, and is maximum around $T_{max}=0.5(T_g+T_m)$.[41] But measurable rates of spherulite growth rate is generally

restricted between T_g+30 K and T_m-10K as a result of thermal motion of polymer chains is conducive to the formation of stable regions between these temperatures.[37] The radial growth rate r of the isotactic polystyrene as a function of the crystallization temperature is shown in Figure 2.20. The radial growth rate first increases and reaches a maximum then falls as the crystallization temperature increases.

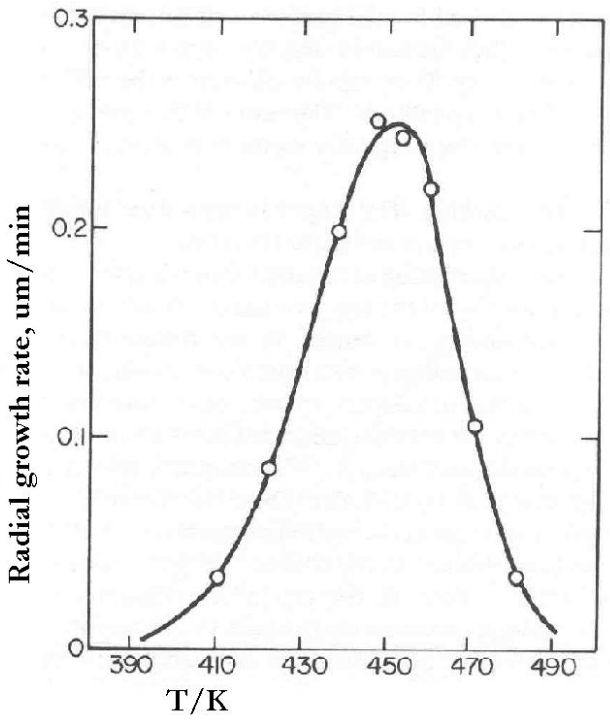

Figure 2.20 : Radial growth rate of spherulites of iPS versus crystallization temperature[37]

Spherulite growth occurs by the simultaneous two-dimensional crystallization of the constituting crystallites.[36,39] Therefore, spherulite growth rate can be used instead of the crystal growth rate *G*. G_{0I}, G_{0II} and G_{0III} in the equations 2.13, 2.14 and 2.15, respectively, show little dependence on the temperature. Thus they can be treated as constants.[45] This assumption enables us to obtain the K_{0I}, K_{0II}, K_{0III} and G_{0i} values with a plot of $LnG + U^*/R(T_c-T_\infty)$ *vs* $1/T\Delta T_c$.[40] These plots are called L-H plots. The common used values for U^* and T_∞ are *1500 cal/mol* and *Tg-30K* for most polymers, respectively.[40,44] Figure 2.21 shows a typical growth rate data and corresponding L-H plot. All the regime transitions may not be observed for every polymer.[40]

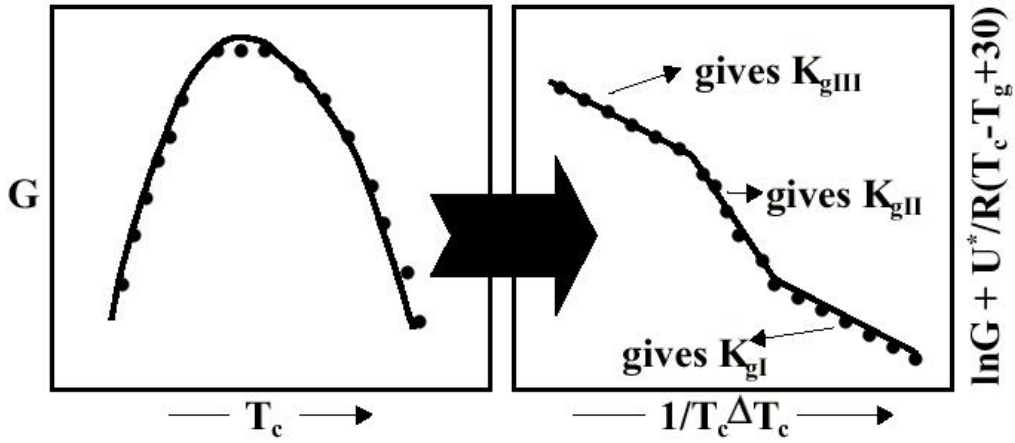

Figure 2.21 : A Schematic diagram illustrating the conversion of growth rate data to L-H plot.[40]

From the growth constants $K_{gI} = K_{gIII} = 2K_{gII} = \frac{4b_0\sigma\sigma_e T_m}{k\Delta H_f}$, the product of the fold and lateral surface energies $\sigma\sigma_e$ can be found.[40] Then since the lateral surface free energy equals:[44]

$$\sigma = 0.1(a_0 b_0)^{1/2} \Delta H_f , \qquad \text{Eq. 2.18}$$

we can determine the value of the fold surface free energy σ_e when a_0, b_0 are known.[44]

2.5.6 Bulk Crystallisation Kinetics and the Avrami Equation

Change of overall crystallinity of the sample over time can be followed by DSC, X-ray diffractometry and dilatometry.[41] When the nucleation of spherulites is assumed to be a Poisson process[41], that is the random distribution of nuclei's in the polymer melt, the change of overall crystallinity of the the polymer can be described by the Avrami Equation where *Q* shows the crystalline fraction[40,41]

$$Q=1-\exp(-Kt^n) \qquad \text{Eq. 2.19}$$

The parameters *K* is usually called bulk crystallization constant and *n* is called Avrami exponent. The bulk crystallization constant *K* depends on the geometry of the growing crystalline entities and amount and type of nucleation. The Avrami exponent

n depends on the geometry and type of the nucleation but does not depend on the amount of the nucleation.[40]

The Avrami equation is simply a mathematical solution of a crystallization model. Here are some examples :[40,41]

i) *N* 2-dimensional discs growing with a constant rate G and nucleated at the same time :

$$Q=1-\exp(-\pi G^2 N t^2)$$

Here $K= \pi G^2 N$ and $n=2$

ii) 2-dimensional discs growing with a constant rate *G* and forming at a rate *N'*

$$Q=1-\exp(-(\pi /3) G^3 N' t^3)$$

Here $K= (\pi /3) G^3 N'$ and $n=3$

In these examples, the growth G is assumed to be only the result of the nucleation at the growth surfaces of the discs. But when other factors like transport of the heat or molecules to the interface, are the rate determining step of the crystal growth, the growth rate can be expressed as $G=(2K/t)^{1/2}$ where *K* is the diffusion constant. The crystal growth *G* is generally constant. As a result, the Avrami exponent may also get some half-integer values. [40,42]

Table 2.2 shows various Avrami exponent values corresponding to different crystal geometries, nucleation types and rate determining steps for the crystal growth rate *G*. In this examples with the Avrami coefficient is either an integer or an half-integer.However in experimental studies, different values are aften reported for n as a result of Avrami analysis.[40,41] This may be as a result of the assumptions in the derivation of Avrami equation. Therefore, the microscopical investigations of the samples are necessary before any interpretation of the Avrami exponent ***n.***[40]

Avrami Exponent	Crystal Geometry	Nucleation Type	Rate Determination
0.5	Rod	Athermal	Diffusion
1	Rod	Athermal	Nucleation
1.5	Rod	Thermal	Diffusion
2	Rod	Thermal	Nucleation
1	Disc	Athermal	Diffusion
2	Disc	Athermal	Nucleation
2	Disc	Thermal	Diffusion
3	Disc	Thermal	Nucleation
1.5	Sphere	Athermal	Diffusion
2.5	Sphere	Thermal	Diffusion
3	Sphere	Athermal	Nucleation
4	Sphere	Thermal	Nucleation

Table 2.2 : Avrami Exponents for various geometries, nucleation types, and rate determining step for crystal growth G[40]

2.6 Supermolecular Structure of iPB-1

Spherulites form when iPB-1 is crystallized from the quiescent melt[14, 43-49] and single crystals are obtained upon crystallization from dilute solutions.[15,16,19,23-25,50] Shish-kebab morphology is also observed when macroscopic shear is applied to a solidifying melt.[34-52]

Monasse and Haudin[44] have studied the morhologies and regimes of growth of two different grades of iPB-1with different molecular weights. They have observed negatively birefringent spherulites from 40 ^{o}C to 110 ^{o}C. Maltese cross of iPB-1 spherulites blurs as the temperature is increased. Above 90 ^{o}C, they have observed that the shape of crystallite entities deviates from sphere. Polyhedrons and squares were seen above 90 ^{o}C. The rate of growth of spherulites were linear and bigger spherulites (crystal entities) formed at higher temperatures. Birefringence of the spherulites also decreases as the temperature is increased. With L-H plots, they have managed to observe all regime transitions of iPB-1. In their work, it was shown that the radial growth rate increases with increasing molecular weight for the two different molecular weight iPB-1 investigated.

Icenogle et.al.[51] have investigated the effect of a wide range of nucleating agents on the crystallization rate of polybutene-1. Most of the additives (Phthalimide, Nylon 11, Polywax 850, Polywax 2000, Alizarin, Quinalizarin e.t.c) enhances the crystallization rate through increasing the number of heterogeneous nucleation. However, some additives decrease crystallization rate. (Anthrone, 9-methyl antharacene, Antharecene, 9-10 dihydro antharacene). The additives decreasing crystallization rate probably acts as a diluent.[51]

Cortazar and Guzman[47] have investigated the effect of molecular weight on the crystallization kinetics of iPB-1. They have obtained fractions with narrow molecular weight distribution. The half-time of the crystallization decreased with increasing molecular weight. In other words, crystallization rate were shown to increase with increasing molecular weight. Spherulite growth rates were also shown to increase with increasing molecular weight. They have also calculated the fold

surface free energy σ_e with L-H plots and the fold surface free energy σ_e were also shown to increase with increasing molecular weight.

Spherulite growth rate of iPB-1 has also been measured in other studies.[14,44-48] Hot stage microscopy were usually employed to measure the spherulite growth rate. Huang et. al.[46] have used a thermal gradient setup that enables to measure the spherulite growth rate for all temperatures at once.

Hot stage microscopy is quite useful for small rates of crystallization. However, when the crystallization takes place in short time interval, hot stage microscopy can not be used since the supercooling rate is small. For this purpose, a liquid medium at T_c can be used for crystallization. [53]

2.7 Applications of Isotactic Polybutene-1

iPB-1 has en excellent creep resistance. Figure 2.22 shows the creep behaviours of some polyolefins compared with iPB-1.[3] Therefore, iPB-1 is an ideal material where creep resistance is the key point. 80 % of the PB-1 is used in pipes.[2] Besides, iPB-1 is used in films and sheets, molding, composites, cables, fibers, and blends.

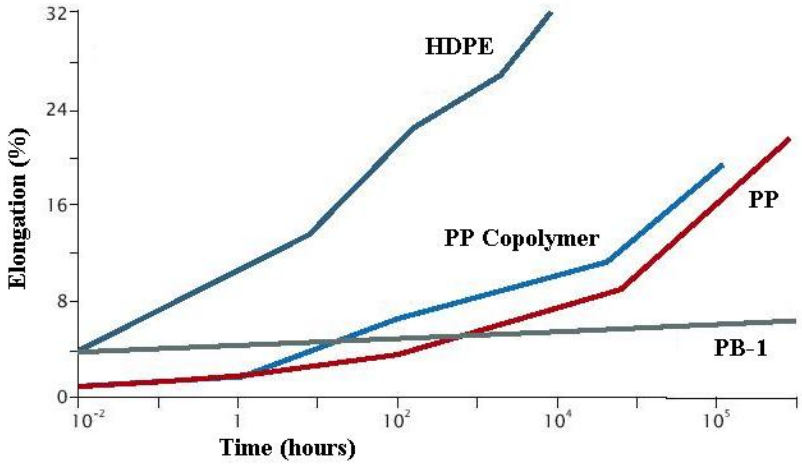

Figure-2.22 : Creep Behaviour of polyolefin resins compared to PB-1. [3]
(Stress = MPa, Temp = 20 ^{0}C)

CHAPTER-3. EXPERIMENTAL PROCEDURE AND THE DESRIPTION OF THE CRYSTALLIZATION CALCULATIONS

3.1 Materials

Four different grades of commercial homopolymers of polybutene-1 were investigated. These materials have been suplied by Shell Research SA (Louvain-la-Neuve, Belgium). These materials are now available from Basell Inc., which is a merger of Shell's and BASF's polyolefins businesses. These grades are isotactic and semi-crystalline exhibiting high creep resistance and environmental stress crack resistance even at elevated temperatures. These are known as PB0110, PB0300, PB0400, and PB0800. Tables 3.1 and 3.2 summarize the densities, the melt flow indices (MFI), the molecular weights and the polydispersities of these four grades investigated. Molecular weights were determined at the Shell Research SA laboratory in Louvain-la-Neuve. Gel permeation chromatography (GPC) was employed to determine the molecular weights. Only PB0110 contains nucleating agents but all contains a heat stabilizer. They are developed for different applications ranging from injection moulding (PB0110, PB0300, PB0400), extrusion (PB0110), blow moulding (PB0110) to adhesives and sealants (PB0800).

Grade	General	Nucleating Agents	Density	MFI (190 ^{0}C/2.16 kg) ASTM D1238
PB0110	**Isotactic Homopolymer**	**Yes**	**0.915 sp gr 23/23 ^{0}C (ASTM D792)**	**0.4 g/10 min**
PB0300	**Isotactic Homopolymer**	**No**	**0.915 sp gr 23/23 ^{0}C (ASTM D792)**	**4 g/10 min**
PB0400	**Isotactic Homopolymer**	**No**	**0.915 sp gr 23/23 ^{0}C (ASTM D792)**	**20 g/10 min**
PB0800	**Isotactic Homopolymer**	**No**	**0.915 g/cm^3 (ASTM D1505)**	**200 g/10 min**

Table 3.1 : The densities and the melt flow indices (MFI) of the investigated PB grades[3]

Grade	M_n	M_w	M_z	Polydispersity
PB0110	**128700**	**854800**	**2497400**	**6.6**
	121900	**847500**	**2449500**	**7.0**
PB0300	**98600**	**391800**	**1038000**	**4.0**
	97500	**405000**	**981800**	**4.2**
PB0400	**81300**	**246400**	**508600**	**3.0**
	82200	**241800**	**502400**	**2.9**
PB0800	**71000**	**194900**	**439500**	**2.7**
	66500	**203200**	**405100**	**3.1**

Table 3.2 : M_n (number average molecular mass), M_w (weight average molecular mass)[1] M_z (z average molecular mass) and the polydispersities (M_w/M_n) of the grades investigated

3.2 DSC Characterization

A Setaram Labsys^{TM} DSC12 was used for measuring DSC thermograms of polymer pellets as received. The pellets weigh from 15 mg to 35 mg. They were sealed in aluminium pans. A heating rate of 2 ^{o}C / min. was applied. Three repeats were carried out for each sample. The melting peaks and the enthalpy of fusion were determined from the thermograms. Crystallinity of the samples determined by enthalpy of fusion of sample divided by the enthalpy of fusion of the Form-I. (Table 3.3) Polymer pellets were assumed to include only Form-I crystals. The enthalpy of fusion of the samples were determined with an Indium reference. The ratio of the integral area per miligram of the sample divided to that of the Indium reference were calculated then multiplied with the enthalpy of fusion of Indium reference.

3.3 FT-IR Measurements

The FTIR spectra were recorded on a BOMEM MB 102 FTIR spectrometer with a resolution of 4 cm^{-1} and 32 scans. 6.1 mg of PB0110 sample was melted between two microscope slides and left for cooling for a few minutes at room temperature and then transferred to the sample holder of the spectrometer. FTIR spectra has been taken after 15min, 30 min, 45 min, 60 min, 90 min, 2h, 3h, 4h, 6h, 12h, and 10days.

3.4 Spherulite Growth Rate Measurements

3.4.1 Microtomy

First 100mmX100mmx8mm plates were compression moulded in the Department of Chemistry, METU (Ankara). The melt temperature used was 200 ^{o}C. Following the compression moulding, a section with dimensions shown in Figure 3.1 was cut from the mouldings for efficient and secure clamping in microtomy. A Shandon Finesse 325 rotary microtome was used to cut thin sections of approximately 10 μm. A disposable steel knife and a 35^{o} of included angle was used in microtomy. The knife and the specimen were maintained at room temperature. The length of the thin sections varied from 4 mm to 10 mm. A soft brush was used to retrieve the sections before they curled and then the samples were sandwiched between two glass

slides with the help of the brush. The aim of using thin films in the experiments are to provide the isothermal cooling of the sample and restrict the spherulite growth in 2-dimensions. Thin films were used so as to provide the isothermal heating of the sample.

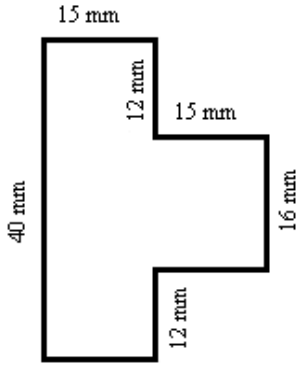

Figure 3.1: Dimensions polymer mould prepared for microtomy

3.4.2 Crystallization Experiments

After microtomy, the samples were melted at 200 ^{0}C ±10 ^{0}C on a hot plate. (Cole-Parmer, VELA, 2000) After keeping the samples for one-two minutes in molten state, they were pressed with the help of a microscope cover slide to remove the air bubbles and obtain a smooth thin film. The samples were kept at this temperature for another 3 minutes to erase any crystallization memory and any flow effects that might have been caused by the cover slide. Then samples were quickly moved to the spherulite growth rate set-up. The stress applied on the samples resulted in films with thicknesses 7±2 μm. The thicknesses of the films calculated with respect to the change of the area of the film.

3.4.3 Spherulite Growth Rate (SGR) Set-up

The Schematic of the spherulite growth rate set-up is shown in Figure 3.2. The SGR setup was placed on the microscope and the growth of spherulites were recorded as a real time movie with the help of a JVC TK01085E CCD camera and a Lifeview^{TM} video capture card connected to a PC. The Microscope used in this work was an Olympus BH2-UMA polarized light microscope The temperature of the setup was controlled with a Cole-Parmer 89000-05 temperature controller and a Cole-

Parmer J-type thermocouple. The crystallization medium was ethylene glycol to provide an efficient cooling of the sample and a good heat transfer. The Figures 3.3 and 3.4 was taken during the experiment. Figure 3.3 shows the set-up, the microscope and the PC. The pictures were taken with a Sony DSC F505V digital camera.

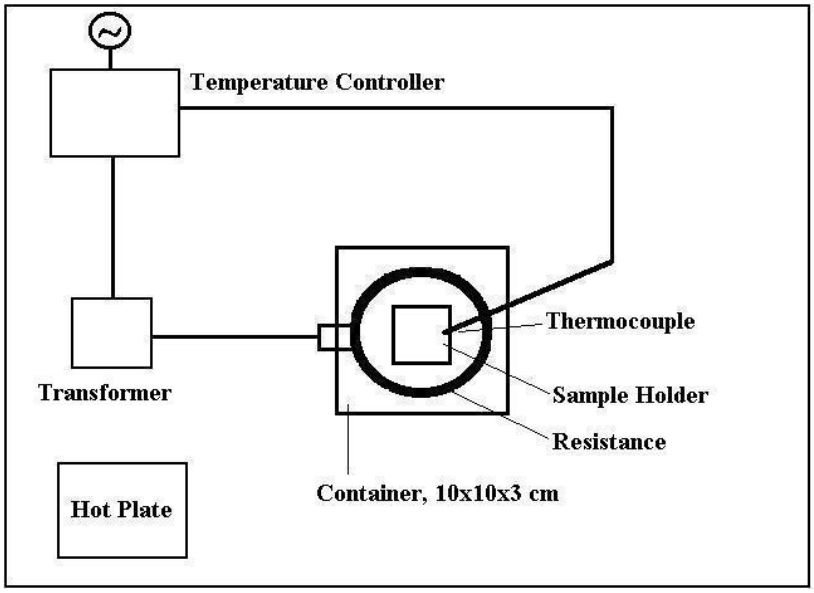

Figure 3.2 : Schematic diagram of SGR set-up

Ethylene glycol is suitable in this study because it is optically inactive and has a high viscosity that prevents wave formation in the bath, which may disturb the image. Water was also tried as a crystallization medium but waves formed on the surface of water due to small vibrations of the set-up preventing the imaging.

Thermocouple of the temperature controller was held very close to the sample holder in the set-up as shown in the Figure 3.4. Even though the temperature difference between any two points might be as high as 3 ^{o}C, the difference between the center of the sample holder and thermocouple was determined to be 0.5 ^{o}C.

The deviation of the temperature from the set temperature was ±1 ^{o}C. In fact the deviation was around ±0.2 ^{o}C when the set-up was kept still. However, since the set-up was moved to see the different regions of the film, the deviation was increased up to ±1 ^{o}C.

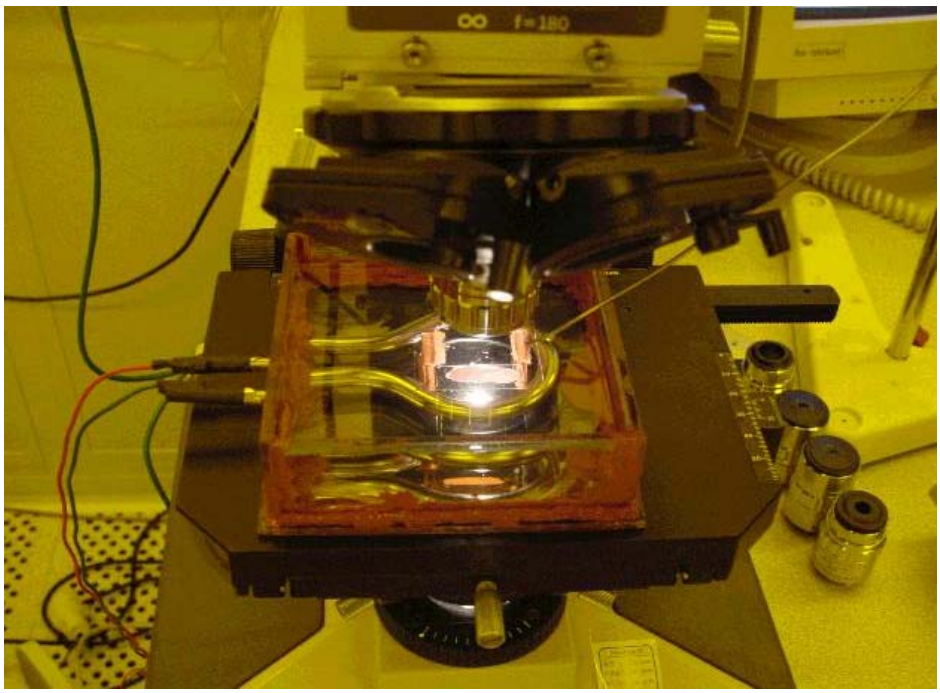

Figure 3.3 : Close-up picture of the SGR set-up

The function of the step-down transformer is to decrease the voltage so that power of the resistance decreases. It is necessary because if the power is too large, the liquid may heat up too fast preventing the temperature controller from operating properly.

Figure 3.4 : Picture of the SGR-setup during the experiment

3.5 The Measurement of Spherulite Growth Rate

Still pictures were obtained from the real-time growth movies of the spherulites and a picture of the graticule with the same resolution and size. Adobe Photoshop 5.0 was used in analysing the still images. The measure tool of the software was used to determine the spherulite size and therefore the spherulite growth rate. Adobe Photoshop Measure tool gives a distance 'D' in cm's if the picture is printed without resizing. This enables us to measure the size of the spherulites provided that they have the same resolution and size.

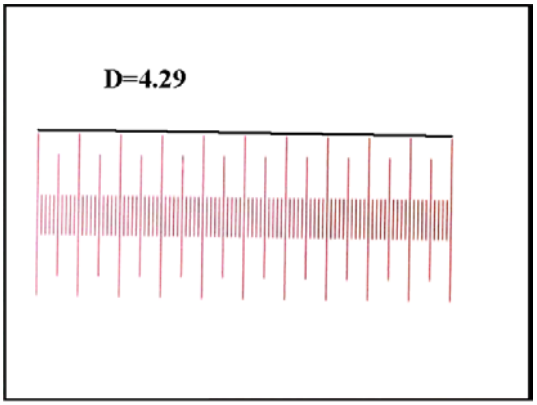

Figure 3.5 :Micrograph of the Graticule with length 1 mm and 100 divisions.

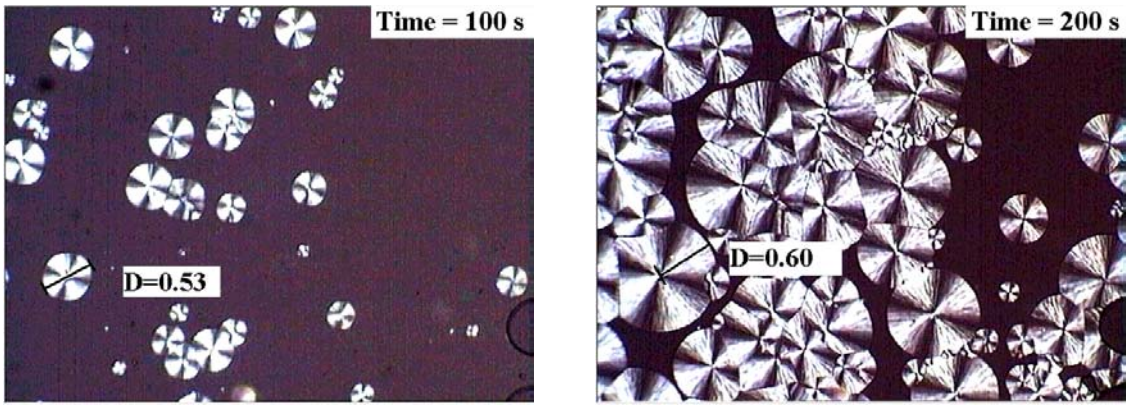

Figure 3.6 : Micrographs of iPB-1 thin films crystallized at 70 ^{o}C. The micrograph on the right is for crystallization time = 100 s and the one the right is for crystallization time = 200 s

From Figure 3.5,

4.29 D = 1000 μm => 1 D = 1000/4.29, 1 D = 233.1 μm, then from Figure 3.6

SGR = r_f-r_i/ Δt = (0.60 – 0.53/2) x 233.1 μm / (200-100) s, =>

SGR= 0.78 μm / s

In the spherulite growth measurements, the size of spherulites were measured for different crystallization times and and radial growth rates were calculated with the least-squares fit of the measured radius as a function of time. Then, the averages of the radial growth rate of samples crystallized at the same crystallization temperatures were used as mean radial growth rate of spherulites at that crystallization temperature.

The measurements give better values at higher temperatures since the size of the spherulites are bigger and the possible errors in the measurements are small relative to increase of the spherulite size. However, at lower temperatures where the size of the spherulites are small, this method may cause some error. For the example given in the previous page, the increase of the spherulite size is from D=0.265 to D=0.60. If the real size of the spherulite were D=0.61 and it was measured as D=0.60, the percentage error for this example would be around 3%. For bigger spherulites thus, the error during the measuring of the spherulite size is smaller, and the error is bigger for the spherulites of the small size, i.e. at low temperatures where the size of spherulites are small.

3.6 Preparation of the L-H plots and Calculation of the Regime Constants

The main theory was already summarised above in section 2.5.5.3. However it is necessary to elaborate on the preparation of the L-H plots since they will often be referred to in the next. From the Equations 2.13, 2.14 and 2.15 :

$$G_i=G_{0i}\, exp(-U^*/R(T-T_\infty))\, exp(-K_{gi}/T_c\Delta T_c), \quad i=1,2 \text{ or } 3 \qquad \text{Eq. 3.1}$$

when we take the natural logarithms of both sides;

$$ln(G_i)=ln(G_{0i})- (U^*/R(T-T_\infty)) -(K_{gi}/T_c\Delta T_c), \quad => \qquad \text{Eq. 3.2}$$

$$ln(G_i) + (U^*/R(T-T_\infty)) = ln(G_{0i}) - K_{gi}\ (1/T_c\Delta T_c) \qquad \text{Eq. 3.3}$$

Equation 3.3 is an equation of $y=A+Bx$ with $y= ln(G_i) + (U^*/R(T-T_\infty))$ and $x=(1/T_c\Delta T_c)$. Therefore, a plot of $ln(G_i) + (U^*/R(T-T_\infty))$ versus $(1/T_c\Delta T_c)$ is linear with the intercept A, which is equal to $ln(G_{0i})$ and with the slope B, being to $-K_{gi}$. Here,

$T_\infty = T_g - 30K$ and $\Delta T_c = T_m^o - T_c$. Then these values of K_{gi} and G_{0I} are used in order to calculate the corresponding growth rate data for the crystallization temperatures and shown in the plots of spherulite growth rate versus crystallization temperature as solid lines. For iPB-1, the values of the U^*, T_g ,T_m^o used in calculations are listed in Table 3.3

Eq. 2.17 states that $K_{gI} = K_{gIII} = 2K_{gII} = \frac{4b_o \sigma \sigma_e T_m^o}{k \Delta H_f}$. So the value of the regime constant from from the L-H plots can be used to find the product of the surface energy term, $\sigma\sigma_e$. Equation 2.18, $\sigma = 0.1(a_0 b_0)^{1/2} \Delta H_f$ enables us to calculate the lateral surface free energy σ, and thus the fold surface free energy σ_e can also be calculated. The values of the $a_0, b_0, \Delta H_f$ are also listed in table 3.3

U^*, activation energy for chain transfer	**1500 cal/mol = 6279 J/mol[44]**
T_g , glass tarnsition temperature	**259 K[45]**
T_m^o, thermodynamic melting point	**406 K[44]**
a_0, the width of the crystalline stem	**0.745 nm[14,44]**
b_0, the thickness of the crystalline stem	**0.745 nm[14,44]**
ΔH_f, enthalpy of fusion of Form-I	**135 J/gram[26]**
ΔH_f, enthalpy of fusion of Form-II	**146 J/gram[26]**
Density of the melt at melting temperature	**0.9 cm^3 [44]**
R, gas constant	**8.31451 J K^{-1} mol^{-1}**
k, Boltzmann constant	**1.38 x 10^{-23} J K^{-1}**

Table 3.3 : The values of variables for iPB-1 used in the calculations

3.7 Calculation of the Overall Crystallization Rates and Avrami Analysis

For the case of two-dimensional growth of the spherulites, the overall crystallinity of the film is directly proportional to the surface area covered by the spherulites. Therefore, the fraction of the surface area covered by spherulites plotted against time for Avrami analysis. The spherulitic regions were cut out from the print-outs of micrographs by a pair of scissors and weighed on a laboratory balance. The ratio of the weight to the total weight of the micrograph is then calculated. Not all the

films are suitable for the measurement of the surface area covered by the spherulites because of two restrictions :

i- At high temperatures, number of the spherulites are so less that there is no impingement of spherulites.

ii- At low temperatures, number of the spherulites are so high that it is not feasible to find the surface area covered.

The Avrami constant and Avrami exponent were determined in a similar way to the determination of the regime constants as explained above. The Avrami equation is :

$$Q=1-exp(-Kt^n), \qquad \text{Eq. 3.4}$$

where Q is the crystalline fraction, or the fraction of the area covered by spherulites at time t. Avrami Equation can also be expressed as :

$$(1-Q)=exp(-Kt^n), \qquad \text{Eq. 3.5}$$

then taking the double logarithm of the both sides :

$$ln(-ln(1-Q))=lnK + n\ lnt\ , \qquad \text{Eq. 3.6}$$

this equation is similar to the $y=A+Bx$ with $A= lnK$ and $B=n$, so a plot of lnt versus $ln(-ln(1-Q))$ gives a straight line with the intercept $A=lnK$ and with the slope $B=n$.

Crystallization half-times were also found by weighing the surface area covered by the spherulites. Crystallization half-time is reached when the surface area covered by the spherulites is the half of the total area.

CHAPTER-4. RESULTS AND DISCUSSION

4.1 Form-II to Form-I transformation by FTIR

FTIR spectra of iPB-1, grade PB0110 is shown below in Figure 4.1. The spectra gained for different ageing times are superimposed. The intensity of the peak at 905 cm^{-1} decreases and the intensity of the peak at the 924 cm^{-1} increases following the ageing at room temperature. The band at 905 cm^{-1} is a characteristic band of Form-II and the band at 924 cm^{-1} is a characteristic band of Form-I. Form-II gradually transforms into Form-I upon ageing at room temperature. In addition, the intensity of peaks at 816 cm^{-1} and 849 cm^{-1} also increases. These peaks are also characteristic peaks of Form-I. Some of the Form-II has already been transformed into Form-I as confirmed with the existence of a peak at 924 cm^{-1} in the scan gained after 14 minutes of ageing. At the end of ten days, the peak at 905 cm^{-1} completely disappears implying that the Form-II to Form-I transformation was complete.

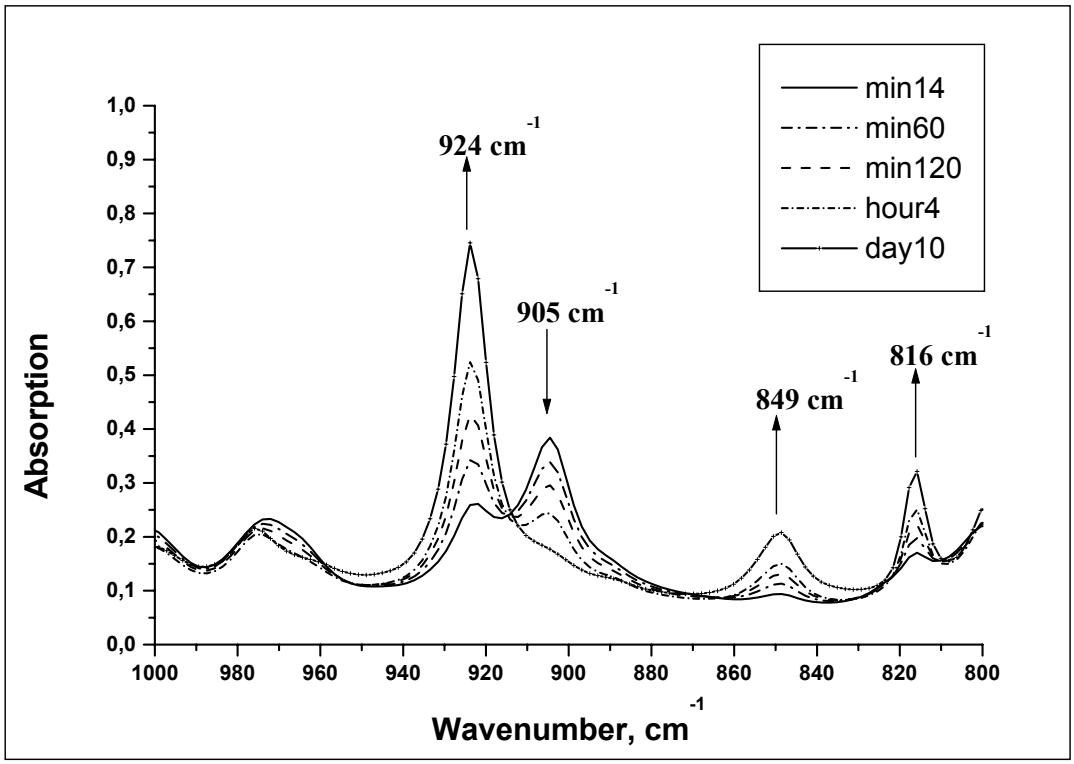

Figure 4.1 : Infrared spectra of iPB-1, 0110 grade vs ageing at room temperature

4.2 - DSC Studies

DSC thermograms of 4 different as received iPB-1 samples were obtained to determine the crystallinities of these grades. The melting peak temperatures, enthalpy of fusions and percent crystallinity of the iPB-1 grades investigated are given in Table 4.1 in the order of decreasing molecular weight.

iPB-1 Grade	Melting Peak, ^{o}C	Enthalpy of Fusion, J/g	Crystallinity,%
PB 0110	**121.5±0.2**	**60.6±1.6**	**44.9±1.2**
PB 0300	**120.3±0.3**	**60.9±3.7**	**45.1±2.7**
PB 0400	**119.5±0.3**	**61.9±3.3**	**45.8±2.5**
Pb 0800	**115.5±0.1**	**58.2±1.5**	**43.1±1.1**

Table 4.1 :Melting peak temperature, Enthalpy of Fusion and percent crystallinity of iPB-1

The melting points decrease with decreasing molecular weight. However, the as-received materials do not exhibit any significant difference in their crystallinities. The crystallinities listed above are very close to the value determined by Starkweather and Jones.[26] They have determined that the crystallinity of the pellets they investigated to be approximately 46 %. 3436115

4.3 Spherulite Growth Rate Studies

4.3.1 Grade PB0110

Grade PB0110 is the grade with the highest molecular weight. It contains nucleating agents to increase the crystallization rate. The radial growth rate of spherulites were determined from 70 ^{o}C to 90 ^{o}C. Below 70 ^{o}C, the nucleation rate and thus the crystallization rate is so high that it is not possible to measure the spherulite growth rate. Figure 4.2 shows the micrographs of grade PB0110 crystallized at 65 ^{o}C, 70 ^{o}C, 75 ^{o}C, 80 ^{o}C, 85 ^{o}C, and 90 ^{o}C. As the temperature is increased, the number of nuclei decreases and therefore their final sizes increase.

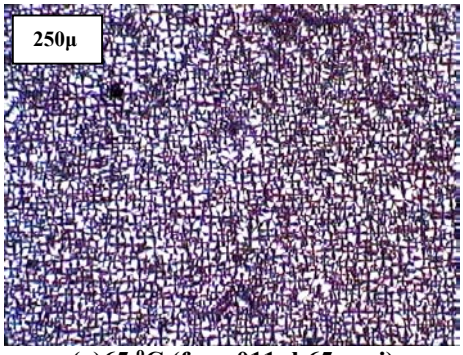

(a)65 ^{o}C (from011pb65c.avi)

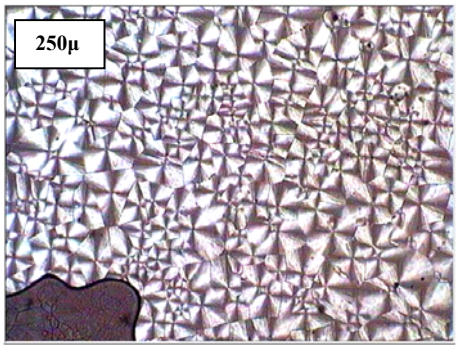

(b)70 ^{o}C (from 011pb70a.avi)

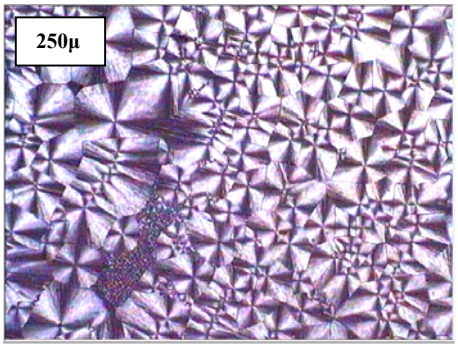

(c)75 ^{o}C (from 011pb75c.avi)

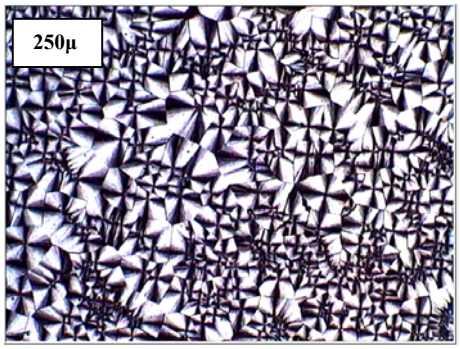

(d)80 ^{o}C (from 011pb80a.avi)

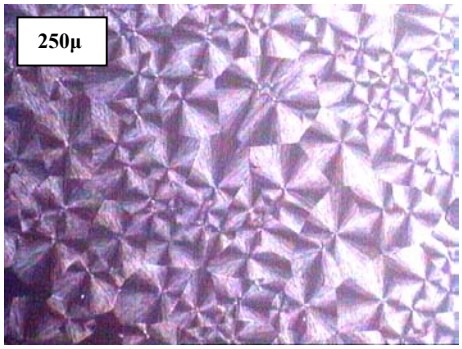

(e)85 ^{o}C (from 011pb85a.avi)

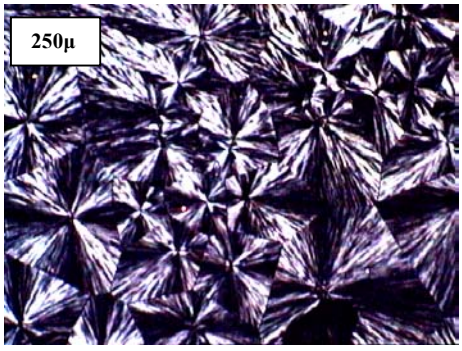

(f)90^{o}C(from 011pb90a4.avi)

Figure 4.2 : micrographs of grade PB0110 film crystallized at different temperatures

Small deviations from spherulitic morphology has only been observed at 90 ^{o}C This is consistent with the observations of Monasse and Haudin mentioned above in section 2.6. The Maltese-cross gets blurry as the temperature increases as shown in Figure 4.2. Black lines are seen in the brighter part of the Maltese cross, which are easily observable in Figure 4.2(f)

Almost all spherulites nucleated at the beginning of the crystallization with some induction time. Therefore the dominant nucleation type is athermal nucleation, Athermal nucleation occurs when melt is supercooled, a nucleus which is not stable at high temperature becomes a stable nucleus upon supercooling of the melt since the critical size of nucleus is small at lower temperatures as discussed above in section 2.5.4.2.3.

The size of spherulites increases linearly with time in this temperature range. Figure 4.3 (a)-(c) shows the growth of spherulites of the grade PB0110 at 90 ^{o}C. This temperature was chosen because the final size of the spherulites is greatest and thus it is easier to follow the growth of spherulites with time. The size of spherulite was plotted against time with a least square fit in Figure 4.3(d)

The growth of spherulites has a negative temperature coefficient, that is the growth rate decreases as the temperature increases as seen in Figure 4.4(a). This implies that the rate determining step in the the growth of the crystal is nucleation, not the transfer of the chains. In some cases, the rate determining step can be the transport of the heat or the molecules to the interface which may lead to the half-integer Avrami exponent *n*. Therefore the Avrami exponent *n* is expected to get integer values only. However, the assumptions in the derivation of the Avrami equation usually results in non-integer *n* values as discussed above in the section 2.5.6.

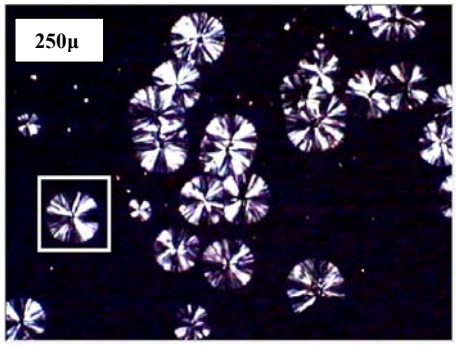

(a) time =20 s

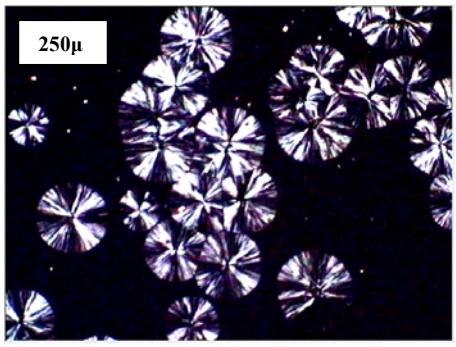

(b) time =100 s

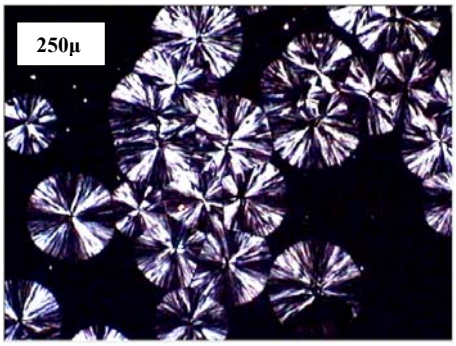

(c) time =180 s

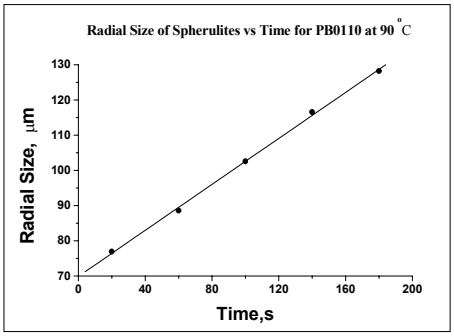

(d)Radial Size vs Time

Figure 4.3 : (a),(b),(c) shows the growth of spherulites of PB0110 at 90 ^{o}C.
(d)Least square fit of the radial size of the spherulite, shown in (a), versus time

The radial growth rate data and the corresponding L-H plot of the PB0110 are shown in Figures 4.4 (a) and (b), respectively. The solid line in Figure 4.4(a) is calculated from Eq. 2.13 with the values of growth constants G and K determined from the intercept and the slope of the L-H plot shown in Figure 4.4(b). (G_{0i}=0.071, K_{oi}= 1.11x10^{5})

The temperature where radial growth rate is maximum could not be determined experimentally for PB0110 due to the presence of nucleating agents.The nucleation density is too high to carry out the necessary measurements. However, the calculated values, the solid line in Figure 4.5 (a), have a maximum at 63.5 ^{o}C. This temperature is important in order to control the mechanical properties of the polymer during processing.

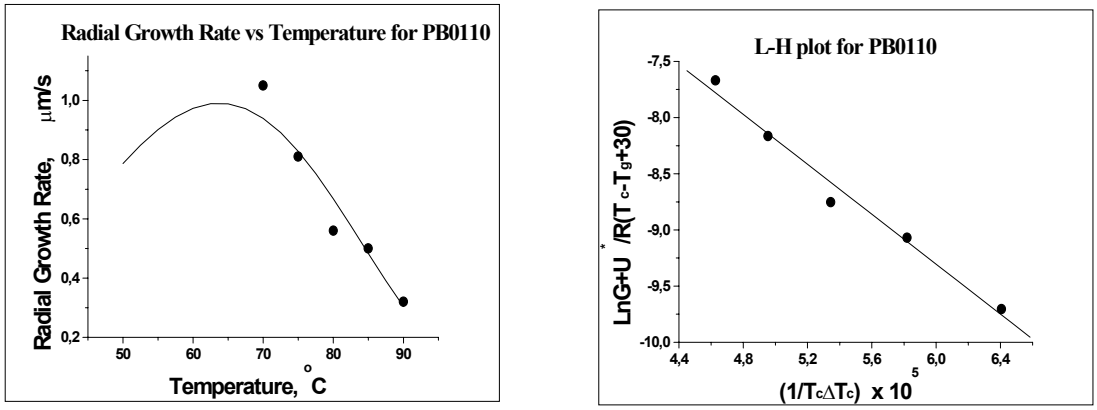

(a) **(b)**

Figure 4.4 : Radial Growth Rate and corresponding L-H plot for PB0110

The linear fit of the growth rate data in the L-H plot implies that the regime of growth is same throughout 70 ^{o}C-90 ^{o}C range. This is also confirmed with the results of Monasse and Haudin.[44] This regime is regime-III, which takes place at lower temperatures. In this regime, the nucleation rate '*i*' is much bigger than the substrate completion rate '*g*'.

The lateral surface free energy σ (the growing surface of lamella) and fold surface free energy σ_e (the large surface of the lamella which can be seen in Figure 2.11) can be calculated from the equations 2.17 and 2.18 as described above in section 3.6. The values of variables used in these calculations are listed in Table 3.3. The values of σ = 10.4 erg /cm^2 (1.04 μJ/cm^2) and σ_e =15.5 erg/cm^2 (1.55 μJ/cm^2)are found. The fold surface free energy σ_e, the surface free energy of the large surface of the lamella (Figure 2.11), carries information about the folding of the chains.

4.3.2 Grade PB0300

Grade PB0300 is the grade with the second highest molecular weight. The radial growth rate of spherulites were determined from 55 ^{o}C to 90 ^{o}C. Below 55 ^{o}C, the nucleation rate and thus the crystallization rate is so high that it is not possible to measure the spherulite growth rate. Figure 4.5(a)-(h) shows the micrographs of grade PB0110 crystallized at 55 ^{o}C, 60 ^{o}C, 65 ^{o}C, 70 ^{o}C, 75 ^{o}C, 80 ^{o}C, 85^{o}C and 90 ^{o}C, respectively.

As in the case of PB0110, the number of nuclei decreases and therefore their final sizes increase from low to high temperatures. Deviations from spherulitic morphology was observed at 90 ^{o}C. The square-like entities were observed at this temperature. This is consistent with the observations of Monasse and Haudin,[44] who investigated two iPB-1 grades with M_n=27,600 and M_n=74600, and polydispersities about 6.5. PB0110 has a M_n around 128,000, for which small deviations from spherical shape have been observed, and PB0300 has M_n around 97,000.

Spherulites have nucleated at nearly the same time upon supercooling after a short induction period for this temperature range (athermal nucleation). Later, a small number of nucleations also occurred giving rise to spherulites with smaller size. However, a high number of secondary nucleations were observed for the sample shown in Figure 4.5(f)

The radial size of spherulites of grade PB0300 grows linearly with time in this temperature range as well. Figure 4.6 (a)-(c) shows the growth of spherulites of grade PB0300 at 80 ^{o}C. Figure 4.6(d) shows the linear fit of the size of the spherulite, which is shown inside a white square in Figure 4.6(a). As in the case of grade PB0110, the growth rate of spherulites decreases with increasing temperature, which means that the rate determining step in the growth of the crystal is the nucleation rather than diffusion.[14] Therefore, the Avrami exponent *n* for PB0300 is also expected to be an integer.

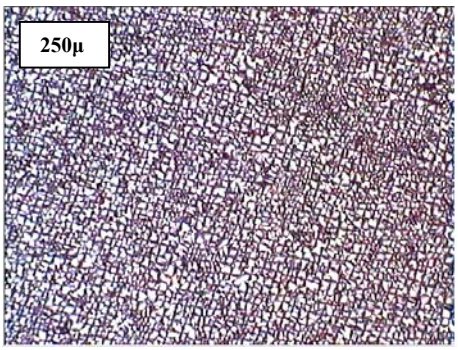

(a)55 °C (from 300pb55a.avi) .

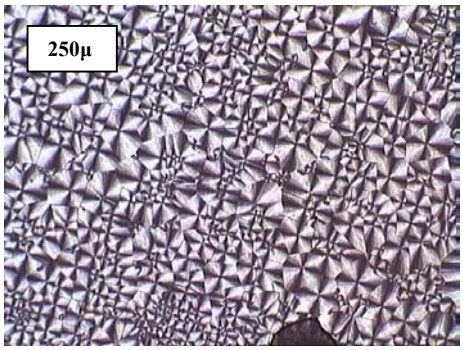

(b)60 °C (from300pb60a.avi)

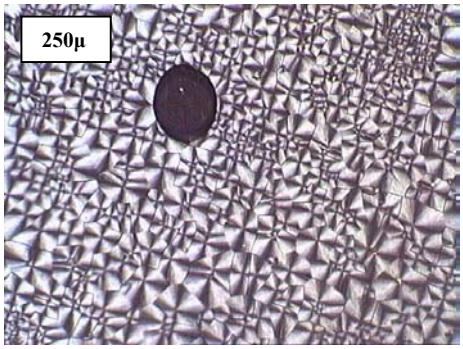

(c)65 °C (from 300pb65a.avi)

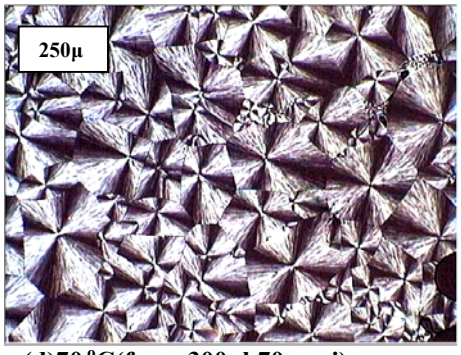

(d)70 °C(from 300pb70a.avi)

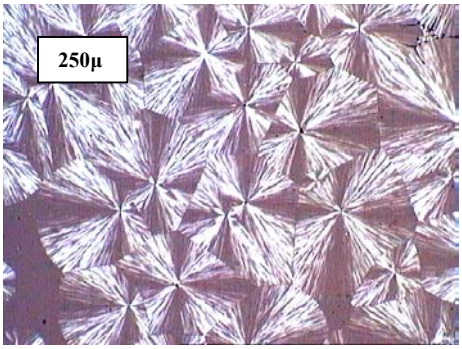

(e)75 °C (from 300pb75c.avi)

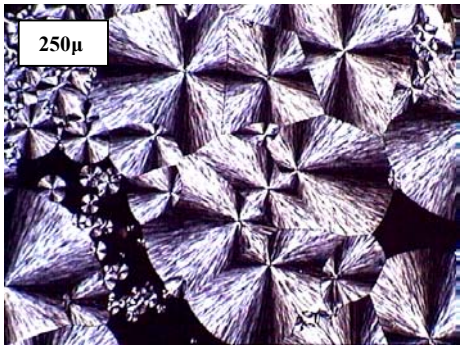

(f)80 °C (from 300pb80a.avi)

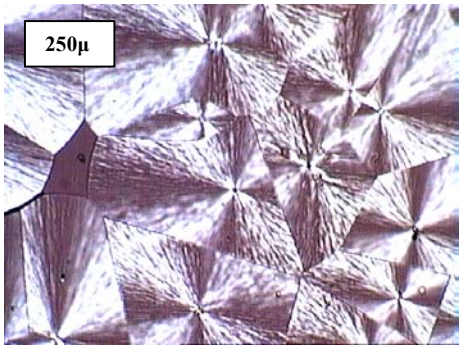

(g)85 °C (from 300pb85a.avi)

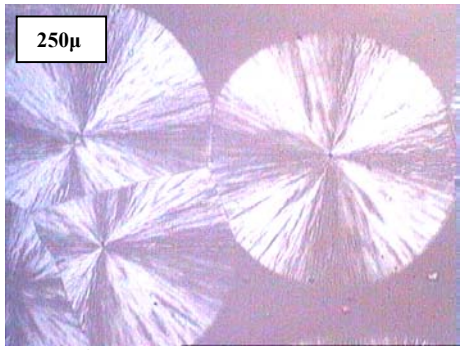

(h)90 °C (from 300pb90a.avi)

Figure 4.5 :Micrographs of grade PB0300 film crystallized at different temperatures

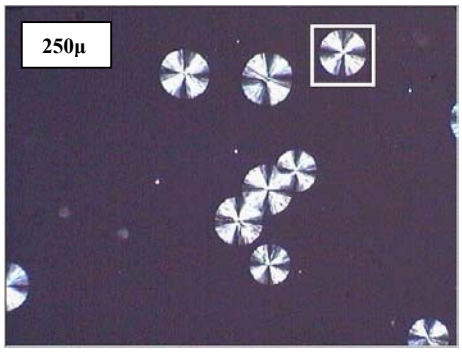

(a) time = 165 s

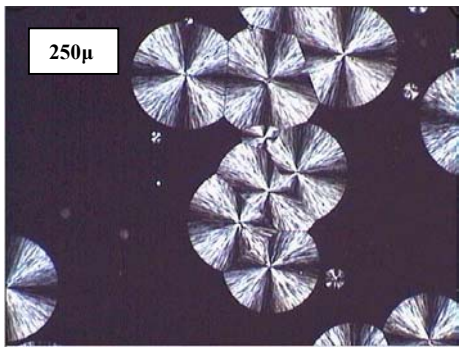

(b) time=338 s

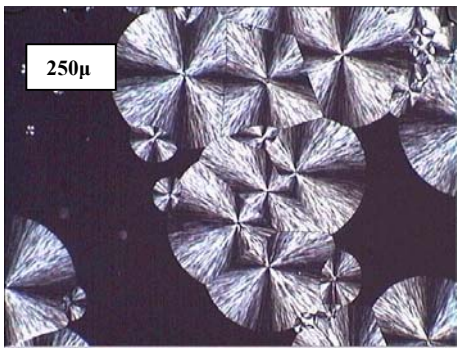

(c) t=455 s

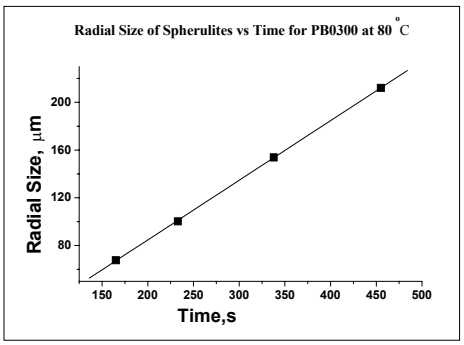

(d)Radial Size vs. Time

Figure 4.6 : (a), (b), (c) shows the growth of sphrulites of PB0300 at 80 ^{o}C
(d)Least square fit of the radial size of the spherulite versus time.

The radial growth rate data and the corresponding L-H plot of the PB0300 are shown in Figures 4.7(a) and (b). The solid line in Figure 4.7(a) is calculated from Eq. 2.15 with the values of growth constants G and K determined from the intercept and the slope of the L-H plot shown in Figure 4.8(b). (G_{0i}=0.113, K_{0i}=1.26x10^5)

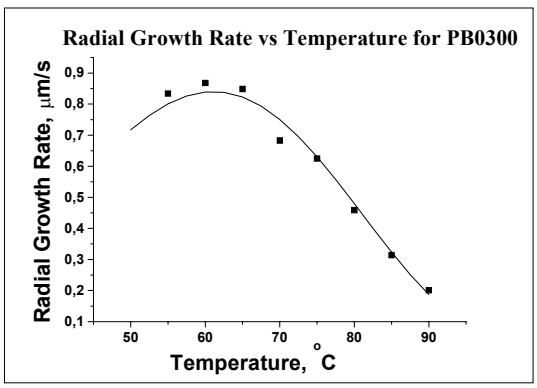

(a)

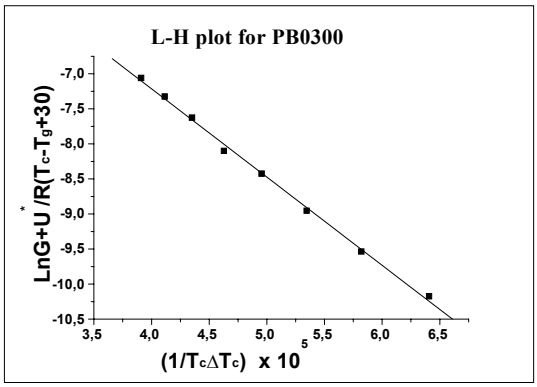

(b)

Figure 4.7 : (a)Radial Growth Rate vs Temperature and (b)corresponding L-H plot.

Experimentally, the radial growth rate maximum was observed at 60 ^{o}C. However, the calculated radial growth rates shown as a solid line in Figure 4.7(a) has a maximum at 61 ^{o}C.

The data lies very close to the linear fit line for the L-H plot shown in Figure 4.7(b).This means that in this temperature range for PB0300, the regime of growth is same as for PB0110, i.e. regime III.

The lateral surface free energy σ was calculated from Eq. 2.18 and thus it is not dependent on the regime constant. Therefore, lateral surface free energy σ=10.4 erg/cm^2 (1.04 μJ/cm^2)is the same for PB0300 as well as for the other grades. The fold surface energy σ_e equals 16.9 erg/cm^2 (1.69μJ/cm^2) from the Eq.2.17 for PB0300.

4.3.3 Grade PB0400

Grade PB0400 has the third highest molecular weight amongst those investigated in this study. The radial growth rate of spherulites of PB0400 were determined from 60 ^{o}C to 90^{o}C. Below 60 ^{o}C, the spherulite growth rate could not be measured due to high number of nucleations similar to the previous grades. Figure 4.8 shows the micrographs of grade PB0400 crystallized at 60^{o}C, 70 ^{o}C, 75 ^{o}C, 80 ^{o}C and 90 ^{o}C. Experiments were also performed 65 ^{o}C,75 ^{o}C and 85 ^{o}C.

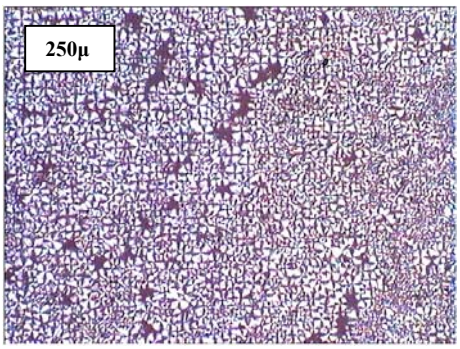

(a)60 ^{o}C (from 400pb60a.avi)

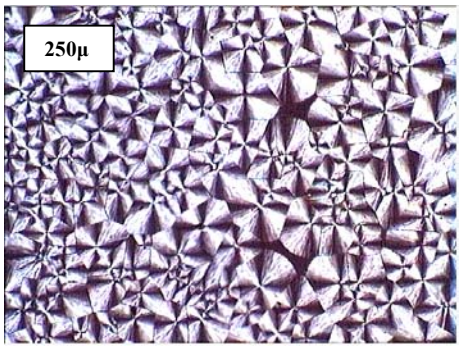

(b)70 ^{0}C (from 400pb70.avi)

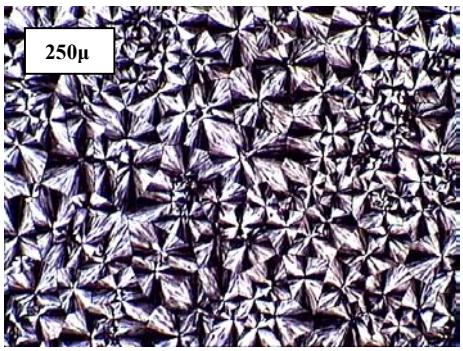

(c)80 ^{o}C (from 400pb80a.avi)

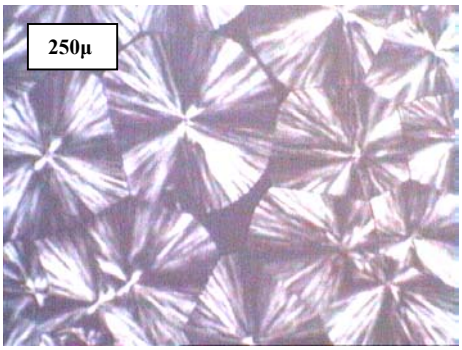

(d)90 ^{o}C (from 400pb90b.avi)

Figure 4.8 : Micrographs of grade PB0400 film crystallized at different temperatures

Like the other grades, spherulites have nucleated almost at the same time with a small number of nucleations occurring later. A deviation of the crystalline entities from a spherical shape has also been observed for the grade PB0400. The first non-spherical crystalline entities are observed at 80 ^{o}C. The corresponding temperature for PB0110 and PB0300 was 90 ^{o}C. For the PB0110, the grade with the highest molecular weight, the deviations from spherical shape was very small.

The crystallization of a polymer over a substrate surface is called epitaxial crystallization. Heterogeneos nucleation, which are due to the foreign particles, is also

called epitaxial crystallization. For all grades, spherulites growing on a dust particle have been observed. The micrograph in Figure 4.9 is a PB0400 crystallized at 90 ^{o}C. An example of the epitaxial crystallization over a dust particle is shown in this figure. Examples of non-spherical crystalline entities can also be seen. In the micrograph. It is worth to mentioning that spherical and sphere-like (non-spherical) crystalline entities can form in the same sample.

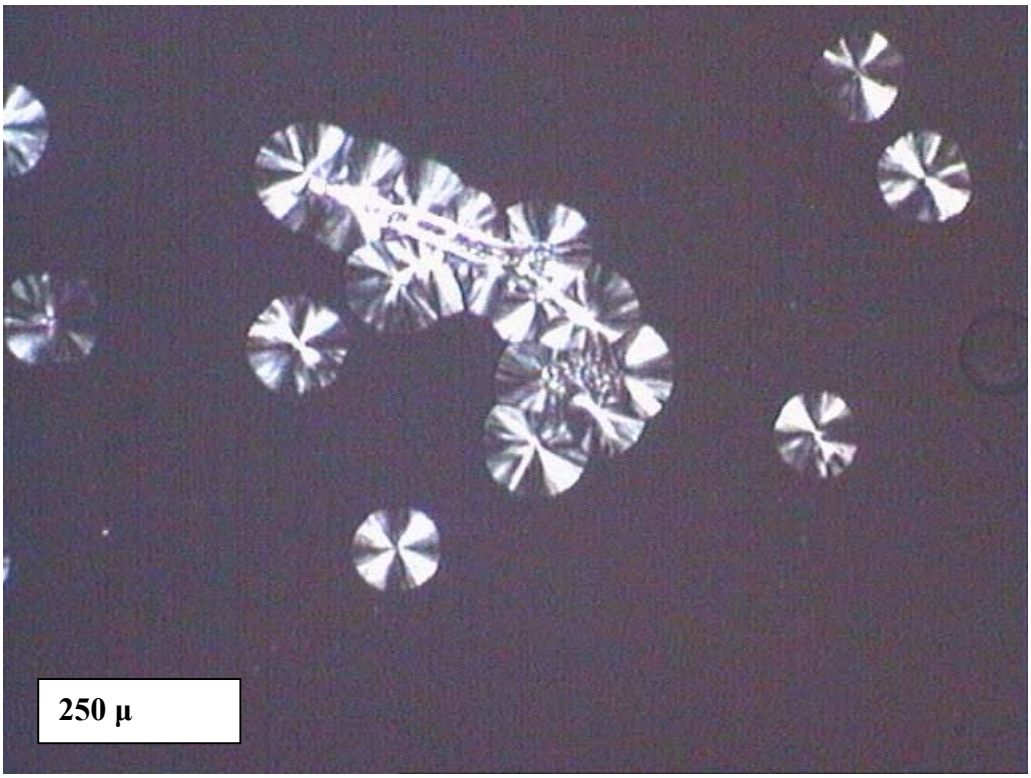

Figure 4.9 :Example of epitaxial crystallization and non-spherical entities. (from 400pb90b.avi)

The radial size of spherulites of PB0400 were also observed to grow linearly in the temperature range observed. Figure 4.10(a)-(c) shows the growth of spherulites of grade PB0400 at 90 ^{o}C. Figure 4.10(d) shows the linear fit for the spherulite size versus time. This particular spherulite taken for measurement is shown within a white square in Figure 4.10(a).

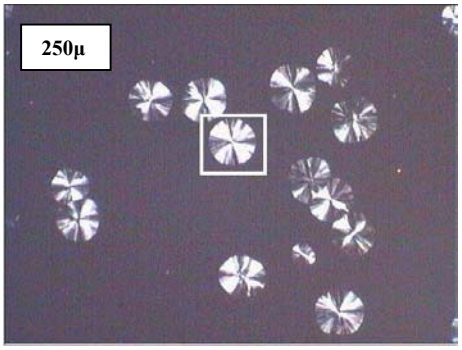

(a) t=430 s

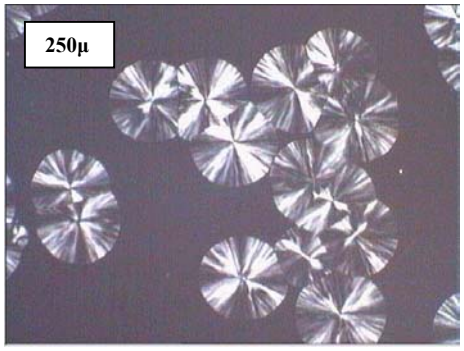

(b) t=746 s

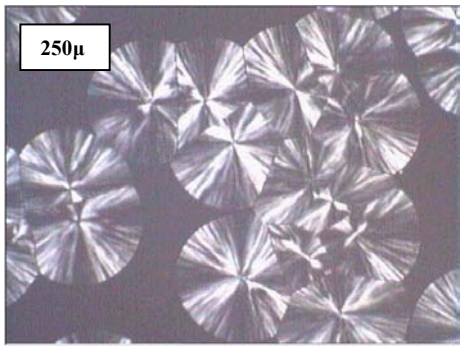

(c) t=1098 s

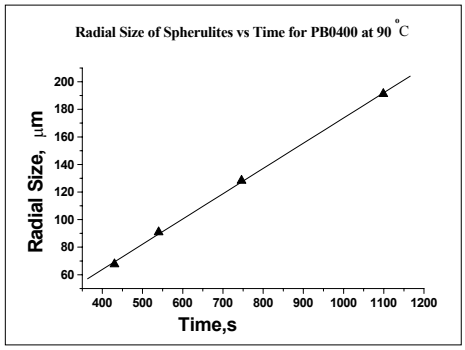

(d)Radial Size vs. Temp.

Figure 4.10 : (a), (b),(c) shows the growth of spherulites of PB0400 at 90 ^{o}C
(d)Least square fit of the radial size of the spherulites versus time.

The radial growth rate data versus temperature and corresponding L-H plot of the PB0400 are shown in Figures 4.11(a) and (b). The solid line in Figure 4.11(a) is the calculated growth rates after the growth constants G and K were determined from the intercept and slope of the L-H plot shown in Figure 4.8(b) (G_{oi}=0.068, K_{oi}=1.17x10^{5}). The growth rate decreases with increasing temperature as seen from Figure 4.11 (a), implying that the rate determining step in the growth of the crystal is the nucleation, not the transfer of chains to the surface or the transfer of the heat.

Experimentally, the radial growth rate maximum was observed at 65 ^{o}C. However, the calculated radial growth rates shown as a solid line in Figure 4.11 (a) has a maximum at 62.5 ^{o}C. In the L-H plot shown in Figure 4.11(b), the data lies very close to the linear fit line. This shows that the data is consistent with the theoretical results and the regime of growth is the same in this temperature range, which is regime III. [44]

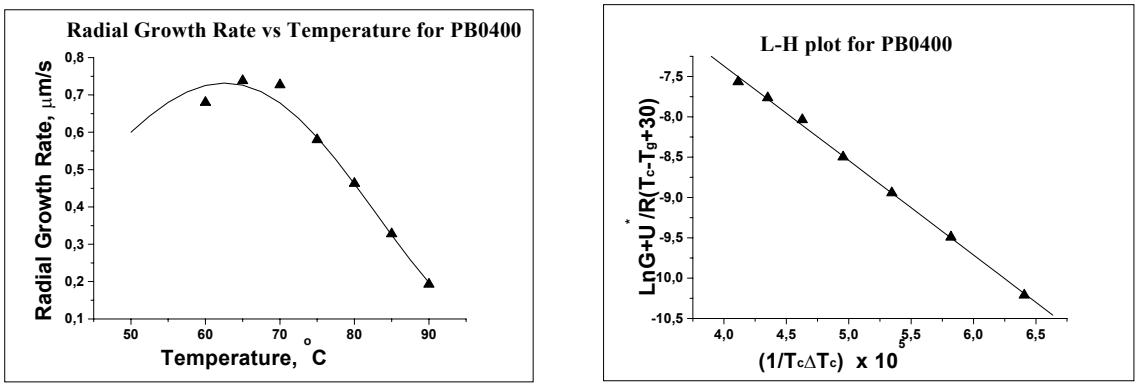

(a) **(b)**

Figure 4.11 : (a)Radial Growth Rate vs. Temperature and (b)corresponding L-H plot

The lateral surface free energy σ equals 10,4 erg/cm^2 (10.4 μJ/cm^2)and the fold surface free energy, calculated by substituting the regime constant K into Eq.2.17, σ_e =15,7 erg/cm^2 (1.57 μJ/cm^2) The fold surface free energy σ_e is directly proportinal to the regime constant K.

4.3.4. Grade PB0800

Grade PB0800 has the lowest molecular weight amongst the grades investigated. The radial growth rate of spherulites were determined from 60 ^{o}C to 85 ^{o}C. Below 60 ^{o}C, the high number of nucleations prevent the accurate measurement of the spherulite growth rate. Figure 4.12(a)-(f) shows the micrographs of grade PB0800 at 60 ^{o}C, 65 ^{o}C, 70 ^{o}C, 75 ^{o}C, 80 ^{o}C and 85 ^{o}C, respectively.

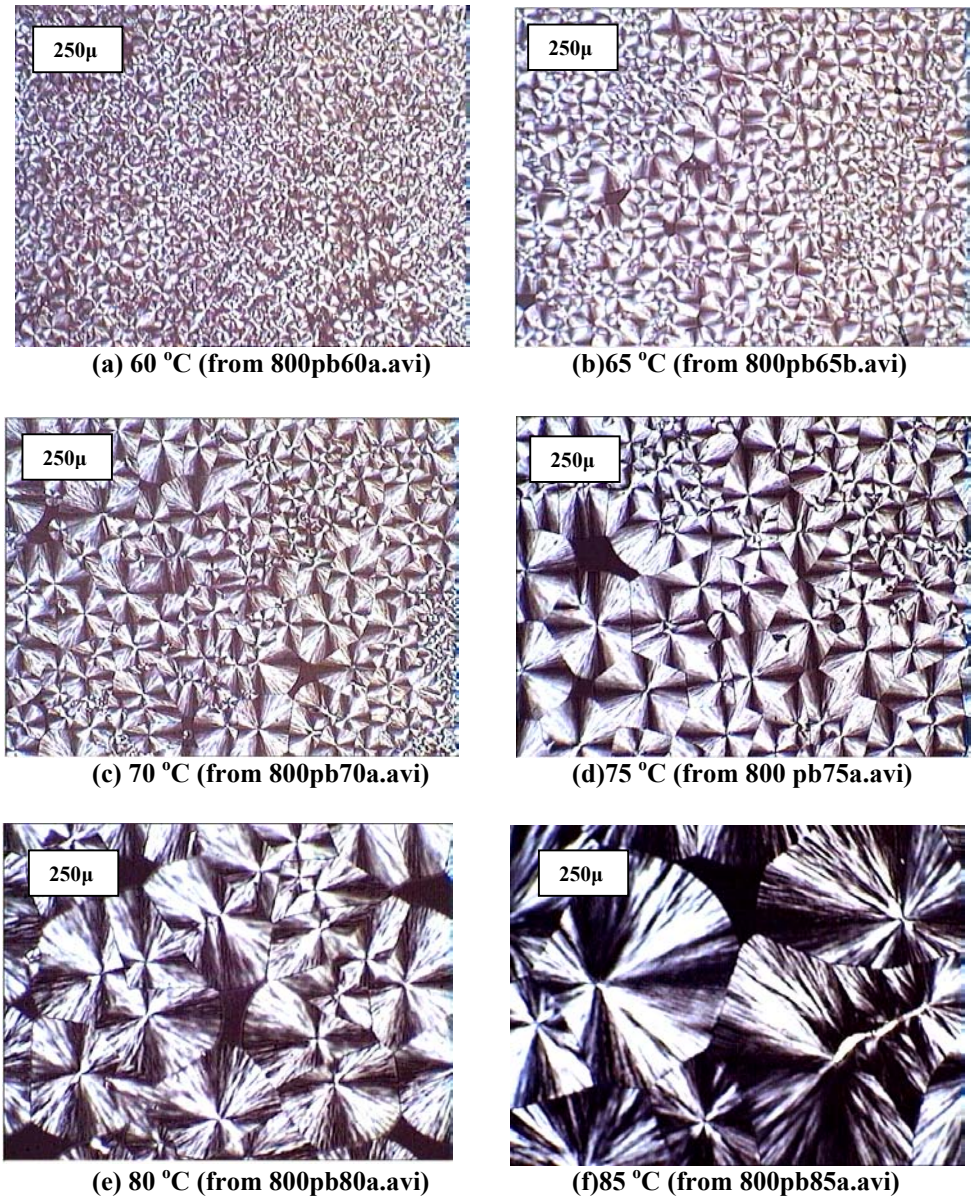

(a) 60 ^{o}C (from 800pb60a.avi) **(b)65 ^{o}C (from 800pb65b.avi)**

(c) 70 ^{o}C (from 800pb70a.avi) **(d)75 ^{o}C (from 800 pb75a.avi)**

(e) 80 ^{o}C (from 800pb80a.avi) **(f)85 ^{o}C (from 800pb85a.avi)**

Figure 4.12 : Micrographs of grade PB0800 films crystallized at different temperatures.

In Figure 4.12 gradual decrease of the number of spherulites and thus gradual increase of the final size of the spherulites can be seen clearly. Deviations from

spherical shape have been observed at temperatures above 80 ^{o}C. The temperature where the deviation from the spherulitic morphology starts was also 80 ^{o}C for the grade PB0400. The deviation from spherical shape has been observed at 90 ^{o}C for the grade PB0110 and PB0300, which exhibit higher molecular weights. The results indicate that the likelihood of deviations from a spherical shape is bigger for lower molecular weight iPB-1 grades.

The nucleations took place in the beginning of the crystallization for PB0800 as well. So for all grades the nucleations were dominated by athermal nuclation giving rise to spherulites with almost the same sizes.

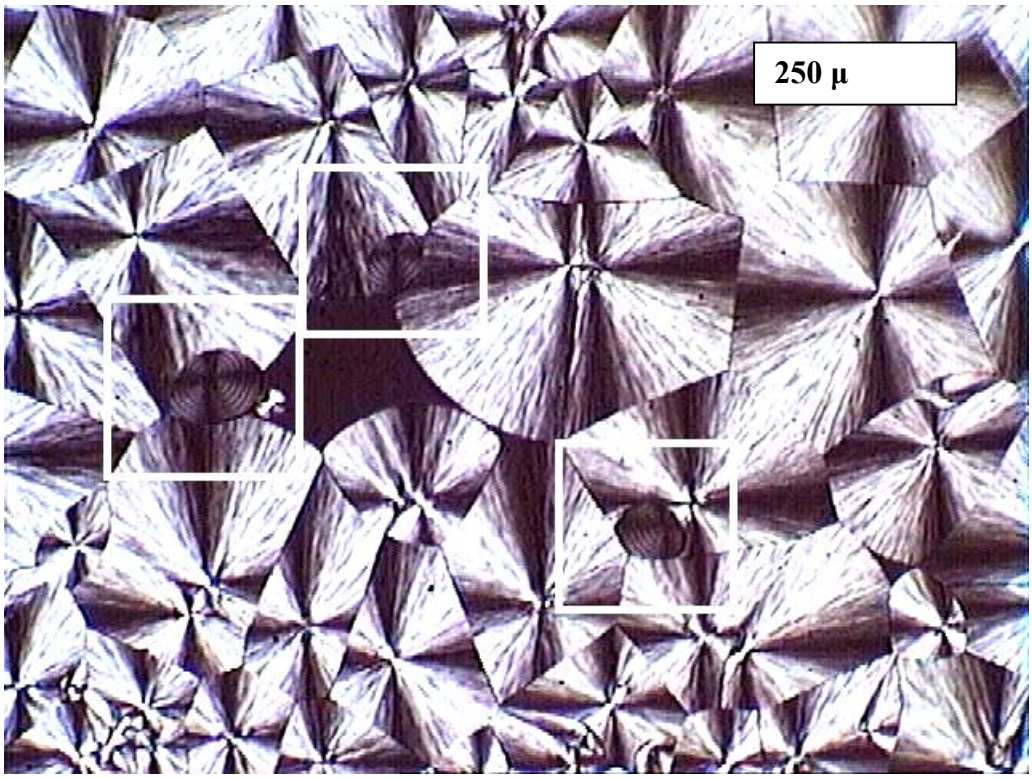

Figure 4.13 : Ringed spherulites formed at 75 ^{o}C for PB0800

Only for one of the samples of PB0800 crystallized at 75 ^{o}C, shown in Figure 4.13, the formation of ringed spherulites have been observed. The formation of the ringed spherulites was not reported in the literature on the crystallization of iPB-1. These ringed spherulites were in the same region of the sample. They have a similar growth rate with the other spherulites and their size is smaller than that of the others, implying that the ringed spherulites have nucleated after the other spherulites.

Like the other grades PB0110, PB0300 and PB0400, the spherulite growth rate is constant during the crystallization of grade PB0800. Figure 4.14 (a)-(c) shows the growth of spherulites of PB0800 at 85 ^{o}C and Figure 4.14 (d) shows the linear fit for the growth of the spherulite shown inside a white square in Figure 4.14(a).

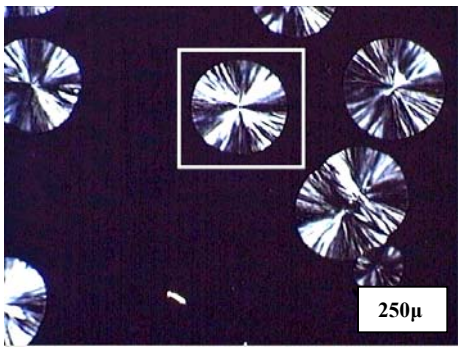

(a) t=666 s

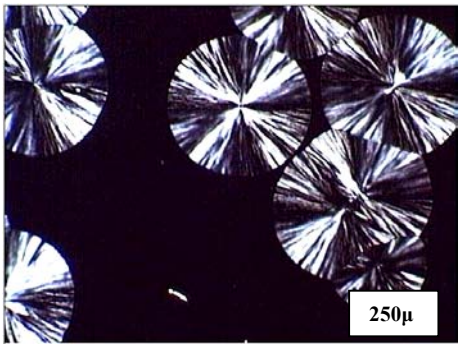

(b) t=959 s

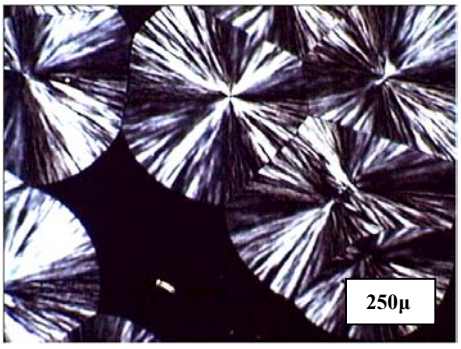

(c) t=1413 s

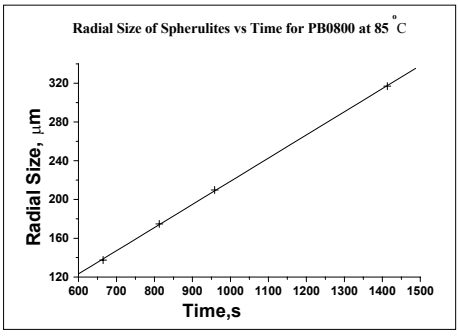

(d)Radial Size vs. Temperature

Figure 4.14 : (a),(b),(c) shows the growth of spherulites of PB0800 at 85 ^{o}C
(d)Least Square fit of the radial size of the spherulites versus time.

The radial growth rate data versus temperature and the corresponding L-H plot of the PB0800 are shown in Figure 4.15 (a) and (b). The solid line in Figure 4.16 (a) is the calculated growth rate values after the growth constants G and K were determined from the intercept and slope of the L-H plot shown in Figure 4.15(b). (G_{0i}=0.105, K_{0i}=1.31x10^{5})

In Figure 4.15 (b), the data lie very close to the regression line, meaning that the data are consistent with the theoretical results and also show that the regime is same throughout this temperature range, i.e regime III. The decrease of the growth rate with increasing temperature means that the nucleation is the rate determining step in the growth of the crystal.

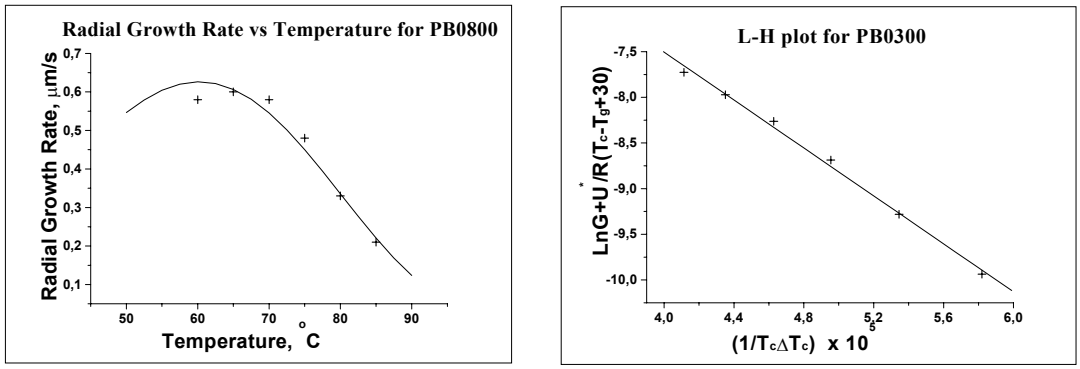

(a) **(b)**

Figure 4.15 : (a) Radial Growth Rate vs. Temperature and (b) the corresponding L-H plot for PB0800

The experimental radial growth rate maximum occurs at 65 ^{o}C, where that of the calculated results are 60 ^{o}C. However, the radial growth rate at 60 ^{o}C (0.58 μm/s) and 65 ^{o}C (0.60 μm/s) are very close to each other in the experiments. The error during the measurement of the spherulite size may cause such a result.

For PB0800, the lateral surface free energy, σ, is 10.4 erg/cm^2 (1.04 μJ/cm^2). Then fold surface free energy σ_e equals 17.4 erg/cm^2 (1.74 μJ/cm^2)from the Eq. 2.18.

4.4 The Effect of Molecular Weight on the Spherulitic Growth Rate

Grade	55 °C	60 °C	65 °C	70 °C	75 °C	80 °C	85 °C	90 °C
PB0110	-	-	-	1.05	0.81	0.56	0.50	0.32
PB0300	0.83	0.87	0.84	0.68	0.62	0.46	0.31	0.20
PB0400	-	0.68	0.74	0.73	0.58	0.46	0.33	0.19
PB0800	-	0.58	0.60	0.58	0.48	0.33	0.21	-

Table 4.2 :Spherulite growth rates for the grades investigated in the order of decreasing molecular weight.

The spherulitic growth rate data for iPB-1 grades are given in the order of decreasing molecular weight in Table 4.2 The spherulite growth rate increases with the increasing molecular weight. The calculated spherulitic growth rate data, or in other words, the fit of Eq 2.13 to this molecular weight are shown in Figure 4.16. Monasse and Haudin,[44] observed similar results for the two grades with different molecular weights. Cortazar and Guzman also[47] got similar results, when they studied the iPB-1 fractions with narrow molecular weight distributions.

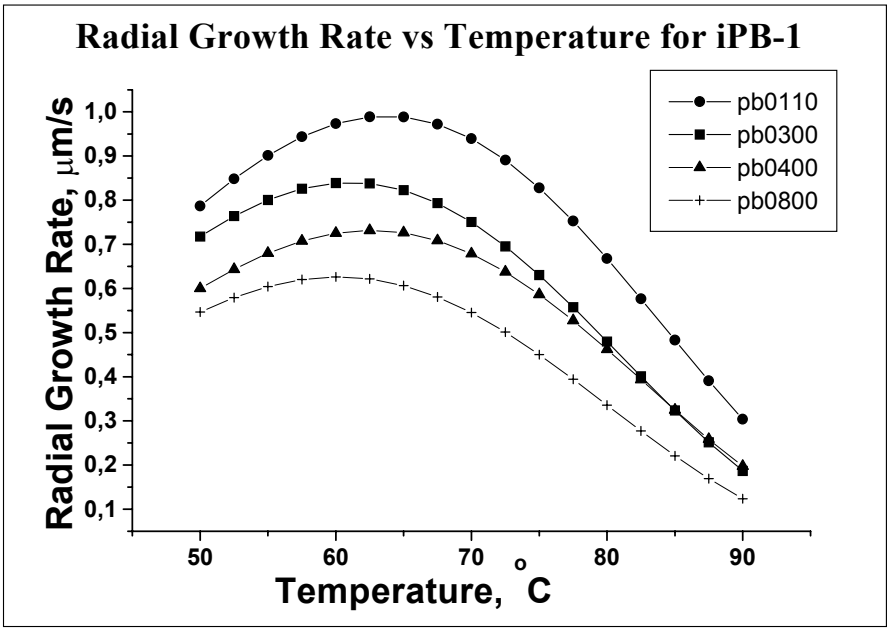

Figure 4.16 : Fit of Eq. 2.13 to the Spherulitic growth rate data for iPB-1 grades

The difference between the spherulitic growth rate of the investigated grades is maximum around the 60 ^{o}C – 65 ^{o}C, where the indivial growth rates are maximum as well. As the temperature increases, the difference decreases. The spherulitic growth rate of the grades PB0300 and PB0400 are almost the same at high temperatures.

Grade	Experimental SGR Maximum	Calculated SGR Maximum
PB0110	**-**	**63.5 ^{o}C**
PB0300	**60 ^{o}C**	**61 ^{o}C**
PB0400	**65 ^{o}C**	**62.5 ^{o}C**
PB0800	**65 ^{o}C**	**60 ^{o}C**

Table 4.3 :The experimental and calculated growth rate maximum for iPB-1 grades

The experimental and calculated temperatures where spherulitic growth rate is maximum is listed in Table 4.3. It should be mentioned that the experiments performed with a 5 ^{o}C interval. These temperatures are important during the moulding of these commercial iPB-1 grades. The mould temperature in processing could be chosen with such crystallization data in mind to obtain products exhibiting the desired mechanical properties. For instance the stiffness (Young modulus) of the samples will be higher for smaller spherulite sizes than larger spherulite size samples. When toughness is important, then the level of crystallization should be kept lower by choosing the appropriate grade of iPB-1

4.5 Effect of Molecular Weight on the Fold Surface Free Energy σ_e

The lateral surface free energies for investigated grades were calculated with Eq. 2.18, which is $\sigma = 0.1(a_o b_o)^{1/2} \Delta H_f$. Thus, it is independent of the regime constant K and equals to 10.4 erg/cm^2 for all grades investigated. Cortazar and Guzman[47] calculated lateral surface free energy σ as 8.3 erg/cm^2 and Powers et. al.[14] found it as 7.3 erg/cm^2 . These values are all close to each other. However, Monasse and Haudin[44] found σ to be 2.7 erg/cm^2. The difference of the results is due to the values of the enthalpy of fusion ΔH_f used in the calculations. We have used the values provided by Starkweather and Jones.[26] They calculated the enthalpy of fusion ΔH_f =146 J/grams. They also cited some other values from the published literature which are all close to their calculated value.Monasse and Haudin[44] determined the enthalpy of fusion by extrapolation of the heats of fusions of the iPB-1 samples crystallized at various temperatures to the melting temperature. Their method is quite a reliable method since it takes into acoount the changes of enthalpy of fusion depending on the crystallization temperature. They have found the enthalpy of fusion of Form-II of iPB-1 as '40 J/g'. It seems that they mixed up the units and used Joule/gram instead of cal/g. If we make this correction, the lateral surface free energy, σ, would equal to 11.3 erg/cm^2, a value very close to our results.

Grade	**σ_e, erg/cm^2**
PB0110	**15.5(1.55 μJ/cm^2)**
PB0300	**16.9(1.69 μJ/cm^2)**
PB0400	**15.7(1.57 μJ/cm^2)**
PB0800	**17.4(1.74 μJ/cm^2)**

Table 4.4 : Fold surface free energy σ_e values calculated in this study

The values of the fold surface free energy σ_e are given in Table 4.4 in the order of decreasing molecular weight. The results are very close to the previous results found by Powers et al.[14](15.5±2.5 erg/cm^2), Monasse and Haudin[44] (19 erg/cm^2 for two iPB-1 grades with different molecular weight), and Cortazar and Guzman[47] (15.4 to 20.5 erg/cm^2). There appears to be another problem with the results of the Monasse and Haudin.[44] They reported both grades with different molecular weights turn to have the same fold surface free σ_e energy of 19 erg/cm^2.

when the regime constants K_{III}=1.13 x 10^{5} for the grade with M_n=27,600 and K_{III}=1.29 x 10^5 for the grade with M_n=74,600 are used from their reported data, σ_e yields different values for different molecular weights. We carried out these calculations by using Eq. 2.17 and 2.18, σ_e values ought to have been reported as 17,3 erg/cm^2 and 15,3 erg/cm^2 for the high and low molecular weight grades respectively. Table 4.5 summarizes the σ_e values from the present study and the values appeared in the published literature.

Reference,	**σ_e, erg/cm^2 or J/cm^{2}x10^{-7}**
Powers et.al.[14]	**15.5±2.5**
Cortazar and Guzman[47]	**15.4 to 20.3**
Monassi and Haudin[44]	**19**
Recalculated (Monasse and Haudin[44])*	**15.3, 17,3**
This Study	**15.5 to 17.4**

Table 4.5 : The comparison of results of this study and the values from the published literature for σ_e.

***Recalculated as explained above**

Cortazar and Guzman[47] observed that the fold surface free energy σ_e increases with increasing molecular weight. However, there was an exception to this rule in the data they presented. They stated that the fold surface free energy, σ_e, increases with increasing molecular weight, then reaches an upper limit. They also cited other published literature showing that such a trend is also observed for other polymers.

However, such a trend is not observed for the results of this study shown in Table 4.4. In our calculations, it is assumed that the thermodynamic melting point is the same for all the grades investigated independent of their molecular weight. However, the thermodynamic melting point is higher for the grades with higher molecular weight. The difference between the thermodynamic melting points of the two iPB-1 grades with M_n =27,600 and M_n=74,600 was found to be around 2.1 ^{o}C by Monasse and Haudin.[44] The thermodynamic melting point has a small effect on the fold surface free energy σ_e through Eq. 2.17 and 2.18. When Eq, 2.18 is substituted into Eq. 2.17 with $a_0 = b_0$ [14,44] and rearranged :

$$\sigma_e = \frac{Kk}{0.4 b_o^2 T_m^o} \qquad \text{Eq. 4.1}$$

So, the change of thermodynamic melting point T_m^o from 130.9 ^oC (404.05 K) to 133 ^oC (406.15 K) effects the fold surface free energy only by 0.5 %.

However, the thermodynamic melting point T_m^o has an indirect effect through the determination of the regime constant K with an L-H plot. The effect of the thermodynamic melting point on the fold surface free energy was studied by Powers et al.[14] The change of equilibrium melting point by 2 K, results in a difference of about 2 erg/cm^2 in the value of the fold surface free energy σ_e. If a higher thermodynamic melting point is used, the fold surface free energy will be higher. Thus, the assumption of the same thermodynamic melting point T_m^o for all the grades with different molecular weight is not very accurate.

The grades investigated in this study have the following approximate number average molecular weights : 125,000 (PB0110), 98,000 (PB0300), 81,000 (PB0400) and 71,000 (PB0800) and with similar polidispersities to the grades investigated by Monasse and Haudin.[44] Thus if the thermodynamic melting points T_m^o differs by 2K between the lowest molecular weight grade and highest molecular weight grade investigated, in a similar way to the results of the Monasse and Haudin,[44] the following results were found, for regime constant K_{III} and the fold surface free energy :

Grade	T_m^0,K	$K_{III,x}10^5K^2$	σ_e,erg/cm^2	T_m^0,K	$K_{III,x}10^5K^2$	σ_e,erg/cm^2
PB0110	**406**	**1.15**	**15.5**	**407**	**1,20**	**16.1**
PB0300	**406**	**1.26**	**16.9**	**406.33**	**1.27**	**17.1**
PB0400	**406**	**1.17**	**15.7**	**405.66**	**1.15**	**15.5**
PB0800	**406**	**1.31**	**17.4**	**405**	**1.26**	**17.0**

Table 4.6 Previous and recalculated values of the regime K_{III} and σ_e

Although it was assumed that the thermodynamic melting points T_m^o of the lowest molecular weight grade and highest molecular weight grade investigated differs by 2K, the actual difference can be even lower. This is because of the fact that

the change of the thermodynamic melting point T_m^o decreases as the molecular weight increases.

The previous observations in the published literature that the fold surface free energy σ_e increases with the increasing molecular weight can be attributed to spherulitic growth rates. The growth of the crystal is faster and the fold surface is more irregular in regime III. As the temperatures increases, the regime-II is observed with a lower crystal growth rate and surface with some irregularities. The growth of the crystal is very slow and the fold surface is very regular in regime I, which takes place at temperatures close to the melting point. Regularity of the surface means that the surface free energy is lower and an irregular surface has a higher surface free energy. Thus, when molecular weight is increased, spherulite growth rate increases and accompanied with a less regular surface and higher fold surface free energy σ_e.

The σ_e values calculated in this study do not exhibit any trend with molecular weight. This does not necessarily disprove the general rule of increasing σ_e with increasing molecular weight. Bearing in mind that the grades under investigation are commercial grades, there may be unreported variations in the chain and chemical structures of different grades i.e. branching and additives which may influence the crystallization behaviour.

4.6 The Avrami Analysis

The Avrami analyses was performed as described above in section 3.7 The results are shown in Figure 4.17. The change of the overall crystallinity versus time and the corresponding fit of the Avrami equation are given in Figure 4.17 (a), (c), (e), (g). The plots of *lnt* vs. *ln(-ln(1-Q)*, are shown in Figure 4.17 (b), (d), (f), (h)

Although a different method, as described above in section 3.7, was used to follow the change of overall crystallization with time, all grades investigated in this study have excellent fit to the in the Figure 4.17. However, the values found for the Avrami exponent *n* are all non-integer values due to the assumptions made in the derivation of the Avrami equation.

The athermal nucleation is the dominating type of nucleation and the rate determing step in the growth of the crystal is the nucleation. for all the grades investigated in this study. Virtually all the crystalline entities formed exhibit circular symmetry. They are either disks or spheres. From the previous studies, it is known that spherical crystalline entities, the spherulites were formed during the crystallization of the isotactic polybutene-1.[14,43-46] Thus according to the Table 2.2, Avrami exponent *n* is expected to be 3. However, Cortazar and Guzman[47] reported an Avrami coefficient n equals 2, indicating a two-dimensional growth of the crystal.

The Avrami exponent n equals 2.72 for PB0110 and 2.79 for PB0800, the values very close to 3. However, for the grades with lower molecular weight, the Avrami exponent n is 2.17 for PB0400 and 2.60 for PB0800. Although the Avrami exponent n deviate from 3 for the grades exhibiting lower molecular weights. However, their overall crystallization rate fits well with the Avrami equation.

In our experiments, the thickness of the films are 7±2 μm, and the diameter of the spherulites ranges from 30 μm to 0.5 mm, and usually being greater than the 100 μm. Thus the growth of the spherulites are first three-dimensional, i.e. spherical, until the diameter of the spherulite equals the thickness of the film, then the growth of the

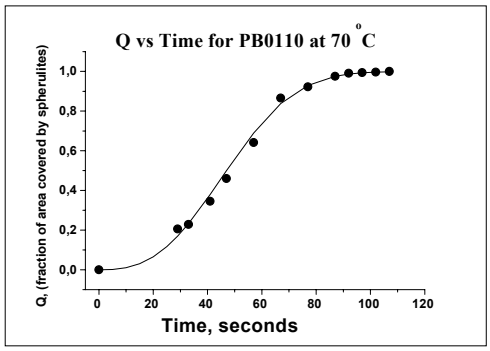

(a)

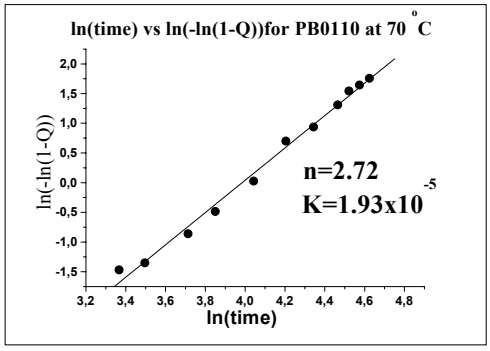

(b)

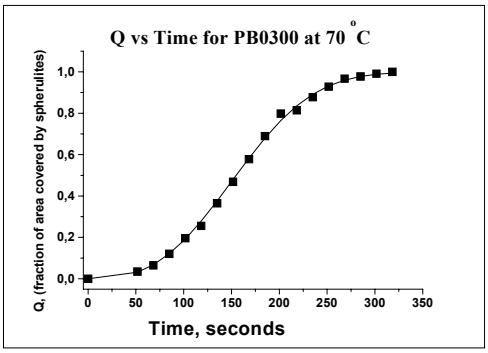

(c)

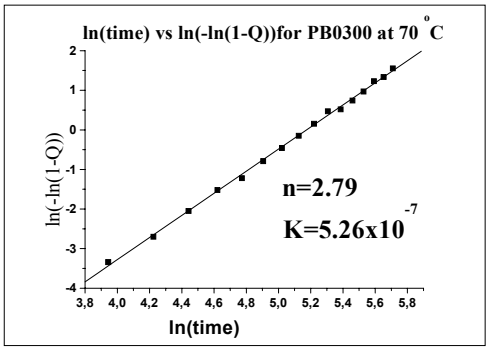

(d)

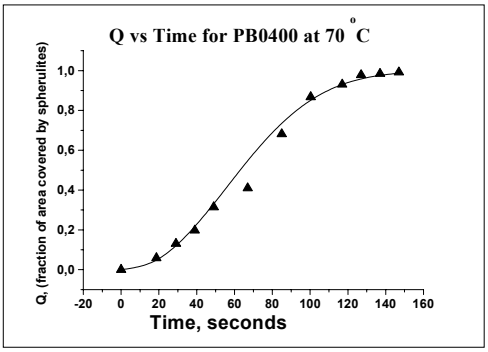

(e)

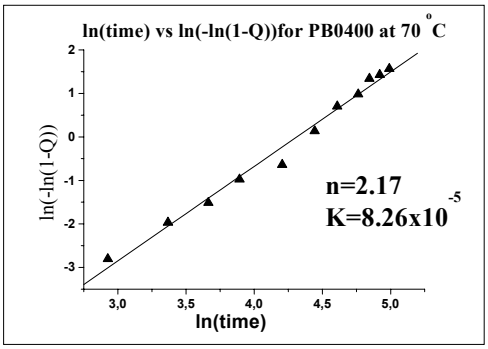

(f)

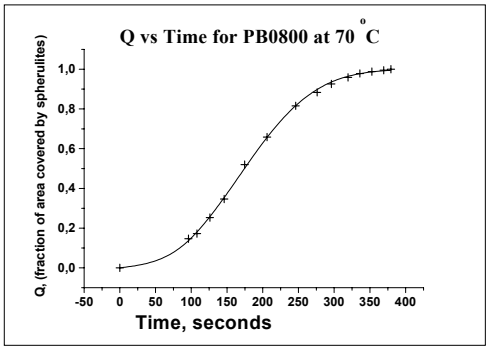

(g)

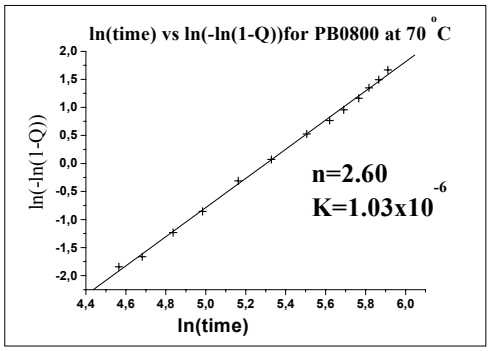

(h)

Figure 4.17 : Avrami analysis and fit of the Avrami equation to overall crystallization change vs. time

spherulite is two-dimensional, i.e. circular. Thus, the results that the Avrami exponent n is always between 2 and 3, can also be attributed to this restriction of the growth to two-dimensions.

4.7 Effect of Molecular Weight on the Overall Crystallization Rate

The overall crystallization rate can be expressed by the half-life $t_{1/2}$ of crystallization, the time when the crystalline fraction is the half of its maximum. In this study, the half-time $t_{1/2}$ was taken as the time when the spherulites cover the half of the area since the area of the spherulites are proportional to the crystalline fraction. Thus, as for the Avrami anaylsis, it can not be applied at the temperatures where the number of the spherulites are so small that only a few spherulites are observed. The half-time of the crystallization for the investigated grades of iPB-1 are listen in Table 4.7

	70 °C	**75 °C**	**80 °C**	**85 °C**
$T_{1/2}$ of PB0110, seconds	**49**	**68**	**72**	**105**
$T_{1/2}$ of PB0300, seconds	**152**	**355**	**358**	**-**
$T_{1/2}$ of PB0400, seconds	**65**	**92**	**126**	**-**
$T_{1/2}$ of PB0800, seconds	**160**	**181**	**344**	**-**

Table 4.7 : Crystallization half-time $t_{1/2}$ of investigated grades

Figure 4.18(a)-(d) shows the micrographs of iPB-1 grades crystallized at 70 °C for 90 seconds. The crystallization of the PB0110 and PB0400 are almost complete. However, a small fraction of the PB0300 and PB0800 are crystallized at this temperature and duration

The crystallization half-time $t_{1/2}$ is inversely proportional to the crystallization rates. Thus the grade PB0110, which contains nucleating agents, has the highest crystallization rate. There is no observable correlation between the crystallization rates and the molecular weights.

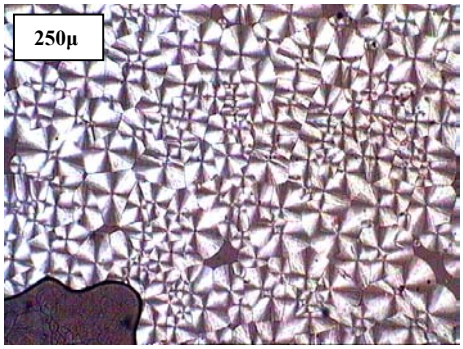

(a)PB0110, 90 seconds

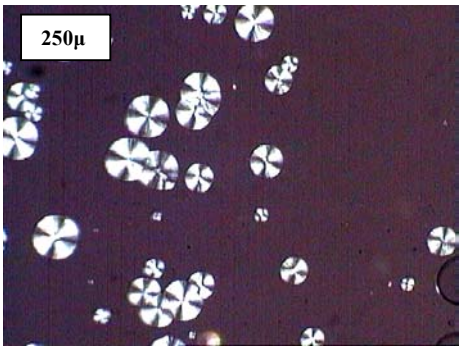

(b)PB0300, 90 seconds

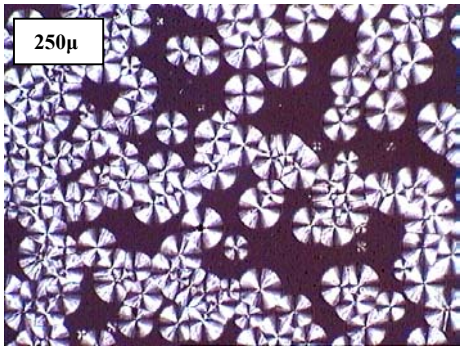

(c)PB0400, 90 seconds

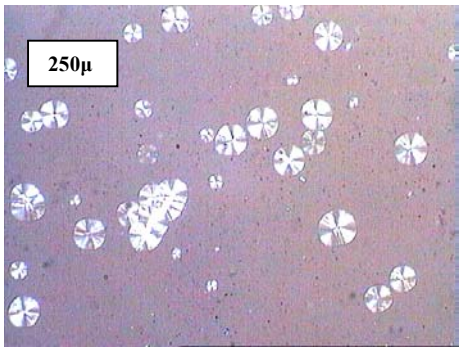

(d)PB0800, 90 seconds

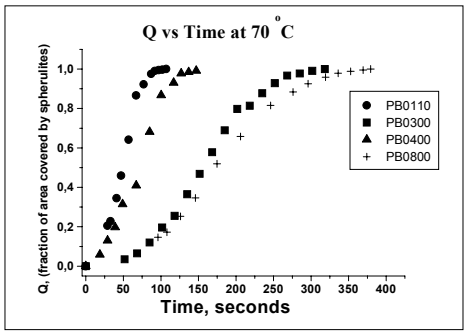

(e)Q vs. Time

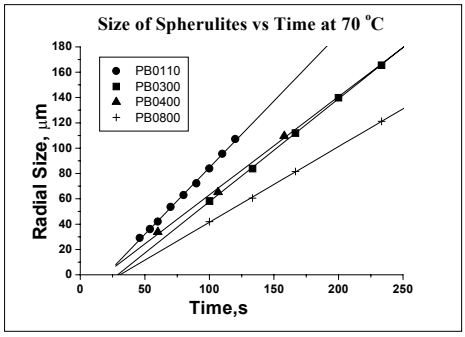

(f)Spherulite Size vs. Time

Figure 4.18: (a),(b),(c),(d) Micrographs of PB0110, PB0300, PB0400, PB0800 crystallized at 70 °C for 90 seconds, respectively. (e) Q vs.Time plots for PB0110, PB0300, PB0400 and PB0800 at 70 °C (f) Spherulite Size vs. time plots for PB0110, PB0300, PB0400 and PB0800 at 70 °C

CHAPTER-5. CONCLUSIONS AND FUTURE WORK

5.1 Conclusions

The conclusions of this research may be summarized as follows:

1-The spherulitic growth rate set-up enables fast cooling of the samples thus the experiments can also be performed at lower temperatures. This is very useful because the real time movie of only one sample is sufficient for a certain temperature instead of quenching very samples for crystallization at different temperatures for varying durations. In previous studies reported in the published literature, where a hot stage microscopy was used for investigation, the experiments were mostly performed over 80 ^{o}C for iPB-1. This is because the spherulite growth rates and crystallization rates are small. The method used in this study provides for an efficient investigation of crystallization kinetics of iPB-1 over a wider temperature range.

2-The radial growth rate of spherulites increases with the increasing molecular weight for the homopolymers of iPB-1 investigated in this study

3-Crystallization rates do not exhibit any dependence on the molecular weight for the grades investigated

4-The lateral and fold surface free energies were calculated and they are very close to the previously reported results. Fold surface free energy does not exhibit any dependence on the molecular weights of the polymers.

5-The grade PB0110, which contains nucleating agents, has the highest crystallization rate.

6-The likelihood of deviation from a spherical shape is greater for the grades with lower molecular weights.

5.2. Future Work

1- The effect of shear on the crystallization behavior of iPB-1 grades should be investigated. The shear can be applied with the help of a glass slide during the crystallization of the films.

2- The effect of film thickness on the spherulitic growth rate of iPB-1 will also be worthy of investigation. Especially the crystallization kinetics of PB-1 films exhibiting thicknesses below 100 nm could be studied.

3- The effect of controlled branching on the crystallization kinetics can be studied with a controlled sythesis of iPB-1 in labarotory.

CHAPTER-6. REFERENCES

1-Shell Chemical Data Sheets

2-L. Luciani, J.Seppälä, and B. Löfgren *Prog. Polym. Sci.* 1988, **13,** 37

3-Polybutene-1, versatility, value and oppurtunity, www.basell.com

url :www.basell.com/pdfs/120.pdf

4-Consice Encyclopedia of Polymer Science and Engineering, / Jacqueline I. Kroschwitz, executive editor. Wiley, New York, 1990

5-Chem expo chemical profile, butene-1, August 16, 1999

url :www.chemexpo.com/news/PROFILE990816.cfm

6-Qigu Huang, Fangming Zhu, Qing Wu, and Shangan Lin. *Polym Int*. 2001, **50**, 45

7-Encyclopedia of Polymer Science and Technology, John-Wiley, New York,1965

8-Hoffman J.D., Miller R.L *Polyme*r 1997, **38,** 3151

9-G.Natta, P. Corradini and I.W.Bassi *Nuovo Cimento*. 1960, **15**, 52

10-Turner-Jones A. *J. Polym. Sci B* 1963, **1**, 455

11-Boor, J. Jr,Mitchell J. C. *J. Polym. Sci B* 1964, **2**, 903

12-Petraccone V., Pirozzi B., Frazki A.Corradini P. *Eur.Polym. J*. 1976, **12**, 323

13-Nakafuku C., Miyaki T. *Polymer* 1983, **24**, 141

14-Powers J. Hoffman J.D. Weeks J.J., Quinn F.A. *J. Res. Natl. Bur Stand.* 1965, **A69**, 335

15-Chau K.W., Geil P.H., *J. Macromol. Sci. Phys.* 1983, **B22**, 543

16-Chau K.W., Geil P.H., *J. Macromol. Sci. Phys.* 1984, **B23**, 115

17-Kopp, S.; Wittmann, J. C.; Lotz, B. *Polymer* 1994, ***3*5**, 908.

18-Kopp, S.; Wittmann, J. C.; Lotz, B. *Polymer* 1994, ***3*5**, 916.

19-Dorset, D. L., McCourt, M. P., Kopp, S., Wittmann, J. C., Lotz,B.

Acta Crystallogr. 1994, ***B5*0**, 201.

20-Mathieu C., Stocker B., Thierry A., Wittmann J.C., Lotz B. *Polymer* 2001, **42**, 7033

21-Winkel A.K., Miles M.J. *Polymer* 2000, **41**, 2313

22-Abenoza M., Armengaud A. *Polymer* 1981, **22**, 1341

23- Kopp S., Wittmann J.C., Lotz B. *J. Mater. Sci*. 1994, **29**, 6159

24-Tosaka M., Kamijo T., Tsuji M., Kohjiya S., Ogawa T., Isoda S., Kobayashi T. *Macromolecules* 2000, **33**, 9666

25-Chau K. W., Yang Y.C., Geil P.H. *J. Mater. Sci.* 1986, **21,** 3002

26-Starkweather Jr H. W., Glover A. J., *J. Polym. Sci. B* 1986, **24,** 1509

27-Geil P. H., Hsu T. -C. *Polym. Commun*. 1990**, 31**, 105

28-Gohil, R. M., Miles, M. J., Petermann, J. *J. Macromol. Sci. Phys.* 1982, **B21**, 189

29-Ullmann's encyclopedia of industrial chemistry executive editor, Wolfgang Gerhartz; senior editor, Y. Stephen Yamamoto ; editors, F. Thomas Campbell, Rudolf Pfefferkorn. 5th Edition.,VCH, New York, 1992

30-Fujiwara Y. *Polymer Bulletin* 1985, **13**, 253

31-Lotz, B.; Mathieu, C., Thierry, A., Lovinger, A. J., De Rosa, C., Ruiz de Ballesteros, O., Auriemma, F. *Macromolecules* 1998, ***3*1**, 9253

32-Samon J.M., Schultz J.M., Hsiao B.S., Wu J. Khot S. *J.Polym. Sci. B.* 2000, **38**, 1872

33-Samon J.M., Schultz J.M., Hsiao B.S., *Macromolecules* 2001, **34**, 2008

34-Kalay G. Kalay C.R. *J. Polym. Sci. B* 2002, **40**, 1828

35-Weynant E., Haudin J.M. *J. Mater. Sci.* 1982, **17,** 1017

36- Billmeyer, Jr. F. W. Textbook of Polymer Science, John Wiley, New York,1984

37- Cowie J.M.G. Polymers: Chemistry and Physics of Modern Materials, Chapman and Hall, New York, 1991

38- Eisele, U. *Introduction to Polymer Physics*, Springer-Verlag, New York,1990

39- Strobl, G. *The physics of Polymers*, Springer-Verlag, Berlin, 1996

40- Ratta V. PhD Thesis, *"Crystallization, Morphology, Thermal Stability and Adhesive Properties of Novel High Performance Semicrystalline Polyimides"*, Virginia Polytechnic Institute and State University 1999

url : http://scholar.lib.vt.edu/theses/available/etd-051799-162256/

41- Kalay G., Private Communications

42- Mandelkern, L. "*Crystallization of Polymers"*, McGraw-Hill, New York, 1964

43- Consice Encyclopedia of Polymer Science and Engineering, / Jacqueline I. Kroschwitz, executive editor. Wiley, New York, 1990

44- Monasse B., Haudin J. M. *Macromol. Chem., Makromol Symp.* 1988, **20/21,** 295

45- Icenogle R.D. *J. Polym. Sci. B.* 1985, **23,** 1369

46- Huang Y., Petermann J. *Polymer Bulletin* 1990, **24,** 649

47- Cortazar M., Guzman G.M. Macromol. Chem.1982, **183,** 721

48- Shaw J.P., Girbert M. *J. Macromol. Sci. Phys.* 1991, **B30**, 271

49- Yang R., Stein R.S. *J. Polym. Sci. A.* 1967, **5,** 939

50- Woodward A.E. *J. Polym. Sci. A.* 1968, **6,** 1987

51- Icenogle R. D., Chatterjee A.M. *J. Appl. Polym. Sci.* 1986, **31,** 1859

52- Kalay G. Kalay C.R. *J. Appl. Polym. Sci.* 2002, in press

53- Stadlbauer M., Eder G., Janeschitz-Kriegl H. *Polymer* 2001, **42,** 3809

54- Dalnoki-Veress K., Forrrest J.A., Massa M.V., Pratt A., Williams A. *J. Polym. Sci. B.* 2001, **39,** 2615